ELSEVIER

Contents lists available at ScienceDirect

BBA - Molecular Basis of Disease

journal homepage: www.elsevier.com/locate/bbadis





BRD9 status is a major contributor for cysteine metabolic remodeling through MST and EAAT3 modulation in malignant melanoma

Ana Hipólito ^{a, b}, Renato Xavier ^b, Cheila Brito ^b, Ana Tomás ^{a, b}, Isabel Lemos ^{b, c}, Luís C. Cabaço ^a, Fernanda Silva ^{a, b}, Abel Oliva ^c, Duarte C. Barral ^a, João B. Vicente ^c, Luís G. Gonçalves ^c, Marta Pojo ^{b, 1}, Jacinta Serpa ^{a, b, *, 1}

- a iNOVA4Health, NOVA Medical School, Faculdade de Ciências Médicas, NMS, FCM, Universidade NOVA de Lisboa, Campo dos Mártires da Pátria, 130, 1169-056 Lisboa, Portugal
- ^b Instituto Português de Oncologia de Lisboa Francisco Gentil (IPOLFG), Rua Prof Lima Basto, 1099-023 Lisboa, Portugal
- ^c Instituto de Tecnologia Química e Tecnológica (ITQB) António Xavier da Universidade Nova de Lisboa, Av. da República, 2780-157 Oeiras, Portugal

ARTICLE INFO

Keywords: Cutaneous melanoma BRD9 Cysteine metabolism Metabolic remodeling

ABSTRACT

Cutaneous melanoma (CM) is the most aggressive skin cancer, showing globally increasing incidence. Hereditary CM accounts for a significant percentage (5–15 %) of all CM cases. However, most familial cases remain without a known genetic cause. Even though, *BRD9* has been associated to CM as a susceptibility gene. The molecular events following *BRD9* mutagenesis are still not completely understood. In this study, we disclosed *BRD9* as a key regulator in cysteine metabolism and associated altered *BRD9* to increased cell proliferation, migration and invasiveness, as well as to altered melanin levels, inducing higher susceptibility to melanomagenesis. It is evident that BRD9 WT and mutated BRD9 (c.183G>C) have a different impact on cysteine metabolism, respectively by inhibiting and activating *MPST* expression in the metastatic A375 cell line. The effect of the mutated BRD9 variant was more evident in A375 cells than in the less invasive WM115 line.

Our data point out novel molecular and metabolic mechanisms dependent on *BRD9* status that potentially account for the increased risk of developing CM and enhancing CM aggressiveness. Moreover, our findings emphasize the role of cysteine metabolism remodeling in melanoma progression and open new queues to follow to explore the role of BRD9 as a melanoma susceptibility or cancer-related gene.

1. Introduction

Cutaneous malignant melanoma (CM) is the malignant transformation of skin melanocytes and the most hostile and invasive among skin cancers, accounting for most skin cancer-related deaths. Increased incidence of malignant CM is directly related to age, with median age of CM onset settled at 64 years [1–3]. Malignant CM aggressiveness is grounded on the higher invasive capacity of CM cells, causing metastatic colonization at early stages and frequent relapse events after primary tumor excision [1]. Importantly, metastasis is reported to decrease median overall survival (OS) of late stage CM patients. Nevertheless, recent studies reported an increase in OS numbers, which is probably a result of the implementation of more efficient therapies and higher clinical surveillance [1,4–8]. Since CM belongs to the group of cancers

that arise due to chronic mutagenic exposure, in this case to ultraviolet radiation (UVR), it is, as expected, one of the tumors that shows the highest mutational frequency [9]. In fact, exposure to UVR is the major known risk factor associated to CM, including natural exposure and tanning bed use, accounting for about 70 % of all CM cases due to extensive genome damage, in a wavelength-dependent manner [2,10–12]. This causes UVR-exposed melanocytes to undergo apoptosis or transformation, losing their initial morphology and function and becoming malignant [11,12]. Other risk factors for melanomagenesis are phenotypical characteristics as fair skin, as well as family history [2]. Hereditary CM covers 5 to 15 % of all CM cases, and is associated with germline mutations in a range of identified CM susceptibility genes [13–20]. However, among all familial CM cases, most remain without an identified genetic cause, which highlights the importance of identifying

^{*} Corresponding author at: iNOVA4Health, NOVA Medical School, Faculdade de Ciências Médicas, NMS, FCM, Universidade NOVA de Lisboa, Campo dos Mártires da Pátria, 130, 1169-056 Lisboa, Portugal.

E-mail address: jacinta.serpa@fcm.unl.pt (J. Serpa).

 $^{^{1}\,}$ Equal contribution.

novel susceptibility genes in hereditary CM [21]. We have previously identified the *Bromodomain-containing protein 9 (BRD9)* as a promising susceptibility gene in the development of familial CM [21]. BRD9 defines different sub-complexes of SWI/SNF [22]. and it works as an epigenetic reader that can selectively identify and bind, through its bromodomain, acetylated lysine residues belonging to histone or non-histone proteins. BRD9, thus, functions as a gene expression modulator by remodeling chromatin and recruiting the transcriptional machinery for certain genes involved in cellular functions, such as proliferation, migration and invasion, as well as metabolic adaptation as the HIF target genes [23], through SWI/SNF(BAF) chromatin remodeling complexes [24–28]. Interestingly, *BRD9* was found to be overex-pressed in several types of cancer [29–33].

In the skin, melanocytes produce the pigment melanin and transfer it to neighboring keratinocytes, where it protects the nuclei content of these cells against UVR-induced damage, acting in a photo protective way by forming supranuclear caps and scavenging absorbed radiation [34,35]. Melanin can be produced in two forms: brownish-black eumelanin and red/orange pheomelanin, the latter associated to the fair skin with a lower ability to tan, freckles and red hair phenotype [36]. The photolability of pheomelanin facilitates the generation of reactive oxygen species (ROS) [37,38], potentiating the mutational character of UVR. It is known that the incidence of skin cancer is directly correlated to skin pigmentation, thus individuals that produce higher levels of pheomelanin are more prone to develop CM [36,39,40]. Both forms of melanin derive, though, from a common precursor: dopaquinone, which is produced from the oxidation of tyrosine by tyrosinase to DOPA and then to dopaquinone [34,41-43]. Eumelanin is then formed by the conversion of DOPAchrome to 5,6-dihydroxyindole-2-carboxylic acid (DHICA) and oxidation of 5,6-dihydroxyindole (DHI) and DHICA, catalyzed by two other tyrosinase-related proteins (TYRP1 and 2) [34,41-44]. On the other hand, pheomelanin is spontaneously produced, requiring only cysteine to form 2, 5- or 5, 5-cysteinylDOPA that leads to the formation of cysteinylDOPA-quinones, and then benzothiazine and benzothiazole [34,41-46]. Besides cysteine, it is known that glutathione (GSH), a tripeptide formed by cysteine, glutamate, and glycine, can further combine with DOPAquinone to form pheomelanin [47,48]. Therefore, the metabolism of cysteine in melanocytes is deeply related to melanin synthesis and its UVR-protective role.

Interestingly, along with the high-rate mutational signature, CM is further described to display metabolic reprogramming features resultant from that mutational status [49]. Metabolic rewiring in crucial pathways such as glycolysis and amino acid metabolism are associated with increased CM malignancy and resistance [49]. However, little is known about cysteine metabolism in CM. In cancer, cysteine metabolic rewiring contributes to a better adaptation of cancer cells to hostile microenvironments, leading to tumor progression and resistance [50]. Rewired cysteine metabolism induces alterations in free radical scavenging and redox maintenance through its antioxidant properties by itself or as a glutathione constituent, altering the detoxifying potential in the microenvironment and constituting a severe chemoresistance mechanism [50–54].

Cysteine metabolic remodeling further interferes in the production of biomass as a carbon source, and in the production of energy as a key player in sulfur metabolism, but also through its reductive catabolism by specific enzymes (cystathionine β -synthase (CBS); cystathionine γ -lyase (CSE), and 3-mercapto-pyruvate sulfurtransferase (MST), the latter working together with cysteine aminotransferase (CAT)) leading to hydrogen sulfide (H₂S) production [55–58]. H₂S, besides working as an antioxidant, can also supply the mitochondrial electron transport chain (mETC), leading to ATP production and so, it is not surprising that H₂S levels are described to impact on cancer cell proliferation and bioenergetics [57,58]. Cysteine uptake occurs through specific transporters and exchangers, as the excitatory amino acid transporter 3 (EAAT3) or the cystine/glutamate antiporter xCT [50]. Both cysteine metabolic enzymes and transporters are described to be overexpressed in several

cancer types [57,59-66].

BRD9, as described above, is a key player in chromatin remodeling, and it can interfere with the action of several transcription factors. Nuclear factor erythroid 2-related factor 2 (NRF2) is a transcription factor described to regulate the expression of antioxidant enzymes (AOEs) [67]. NRF2 binds to specific DNA regions designated by antioxidant responsive element (ARE) sequences, which are conserved genomic regions, involved in orchestrating cellular responses to oxidative stress, maintaining cellular redox balance [68]. Moreover, NRF2 has been described to regulate the SCL1A1 expression encoding the excitatory amino acid transporter 3 (EAAT3), which is able to transport cysteine [69]. The role of SWI/SNF and BRD9 in NRF2 action is controversial and it seems to be tightly dependent on the cellular and disease context. In NSCLC, the loss of function of SWI/SNF, is associated with the activation of NRF2/KEAP1 pathway [70]. However, some SWI/ SNF sub complexes can also potentiate the expression of NRF2 target genes [71], in renal cell carcinoma. Furthermore, in chronical lymphocytic leukemia, the expression of NRF2 and downstream targets are significantly decreased upon BRD9-silencing [72].

Our previous BRD9 study was dedicated to a familial melanoma cohort and no statistical association was found. However, this can be due to the relatively small number of individuals analyzed and the low representativeness of cancer stages. Nevertheless, BRD9 can be targeted by somatic mutations in sporadic melanoma. Therefore, our study aims to analyze the putative regulatory role of *BRD9* in cysteine metabolism remodeling to disclose metabolic phenotypes contributing to CM aggressiveness. We verified that A375 cell line aggressiveness correlates with the overexpression of MST and EAAT3, and disclosed a putative mechanism linking mutated forms of *BRD9* to susceptibility to melanomagenesis.

2. Materials and methods

2.1. Biological samples and institutional approval

DNA samples from patients with multiple primary CM (n=25), indexes with familial CM (n=42) and relatives without CM (n=5), diagnosed at IPOLFG were used in this study. The Familial Risk Clinic from IPOLFG monitored all participants that were subjected to genetic testing according to the current criteria used in Portugal [73]. The clinicopathological data of 72 Portuguese patients, which tested negative for pathogenic germline mutations in high/intermediate-risk CM susceptibility genes (CDKN2A, CDK4 and MITF), is presented in Table S1. DNA was extracted from leukocytes and quantified using QubitTM Fluorometer (Thermofisher) as described elsewhere [21]. This study was approved by the IPOLFG Ethics Board Committee (UIC/829), and written informed consent was obtained from all patients.

2.2. In silico analysis

The potential impact of *BRD9* rare single nucleotide variants (SNVs) on protein function and/or splicing signals was assessed using 30 predictive programs. Since all identified SNVs were reported in public genome databases, most of pathogenicity prediction scores were available in distinct platforms, including Ensembl, Catalogue Of Somatic Mutation In Cancer (COSMIC), Varsome and Franklyn by Genoox. To complete the *in silico* analysis, MutationAssessor, Protein Variation Effect Analyzer (PROVEAN), Cancer Genome Interpreter, MutationTaster2021, Human Splicing Finder, IntSplice2, Functional Analysis through Hidden Markov Models (FATHMM) (including MKL- and XF-based algorithms) and Combined Annotation Dependent Depletion (CADD) were used [74–84].

2.3. Cell line culture

Human malignant melanoma cell lines A375 (American Type Culture

Collection (ATCC), CRL-1619) and WM115 (Rockland code WM115-01-0001, BRAF V600E mutated, USA) were cultured according to the supplier's instructions. We choose to use two cell lines with different levels of aggressiveness to test the impact of the expression of BRD9 WT and Mut variants, bamely A375 (more invasive) and WM115 (less invasive). Both cell lines were maintained in Dulbecco's Modified Eagles Medium (DMEM) (41965-039, Life Technologies), supplemented with 10 % fetal bovine serum (FBS) (S 0615, Merck), 1 % Antibiotic-Antimycotic (AA; P06-07300, PAN Biotech) and 50 $\mu g/mL$ Gentamicin (15750-060, Life Technologies). Cell cultures were maintained at 37 °C in a humidified environment of 5 % CO₂. Cells were detached with 0.05 % Trypsin-EDTA $1\times$ (25300-054, Thermo Fisher Scientific) at 37 °C for approximately 5 min and split to new plates according to the experimental standard procedures. Cells were metabolically synchronized under starvation prior to the exposure to experimental conditions.

2.4. Primary cell culture

Human epidermal keratinocytes isolated from neonatal foreskin (HEKns) (C—0015C, Thermofisher) were cultured in EpiLife medium (M-EPIcf-500, Gibco) supplemented with 1 % commercial mix of human keratinocyte growth factors (S-001-5, Gibco), 0.06 mM calcium chloride (J62905.K2, Gibco) and 1 % PenStrep (15070063, Gibco). Human dermal fibroblasts isolated from neonatal foreskin (HDFns) (C-004-5C, Gibco) were grown in DMEM (11960, Gibco) supplemented with 10 % FBS (10500064, Gibco), 2 mM L-alanyl-L-glutamine dipeptide (35050038, GlutaMAX, Gibco) and 1 % PenStrep (15070063, Gibco). HEKn were used until passage 4 and HDFn until passage 13. Both HEKns and HDFs were grown in a humidified incubator at 37 °C with 5 % CO₂.

2.5. BRD9 overexpression and BRD9 c.183 G>C transfection

A375 and WM115 cell lines were transfected with three distinct expression plasmids: pCMV6-Empty (CAT# PS100001, Origene Technologies), pCMV6-BRD9 WT (CAT# RC229303, Origene Technologies; BRD9 - NM_023924 - Human Tagged ORF Clone) and pCMV6-BRD9 c.183G>C (CAT#CW305250, Origene Technologies). pCMV6-BRD9 c.183G>C contains the mutant open reading frame of RC229303 at nucleotide 183 from G to C leading to a E61D amino acid change. The transfection was performed with Lipofectamine 2000 Transfection Reagent (11668019, Thermo Fisher Scientific), following manufacturer's instructions. Stable transfected clones expressing neomycin resistance marker were selected using 1500 μ g/mL of G-418 geneticin (10131035, Thermo Fisher Scientific). Validation of transfection was confirmed using Sanger sequencing, reverse transcription and quantitative real-time PCR and western blot, as described.

2.6. Sanger sequencing

The mutational status of all *BRD9* exons in the IPOLFG cohort of familial CM was evaluated by Sanger sequencing, as described elsewhere [21], using specific pairs of primers for each exon, represented in Table 1.

Validation of transfection of A375 and WM115 cell lines, using cDNA, was performed upon amplification by PCR and Sanger sequencing, using forward 5' ACGAGGATTATGCCGACAAG 3' and reverse 5' CGTCCAGATGCTTCTCCTTC 3' primers, and the protocol proposed by Big DyeTM Terminator v1.1 Cycle Sequencing RR-100 Kit (4336768, Thermo Fisher Scientific). Afterwards, samples were purified using Exonuclease I 20 U/µl (EN0582, Thermo Fisher Scientific) and FastAP Thermosensitive Alkaline Phosphatase 1 U/µl (EF0654, Thermo Fisher Scientific), and analyzed in an automatic sequencer 3500 Genetic

 Table 1

 Primers used for BRD9 exons amplification. Detailed characterization of the primers used in Sanger sequencing for BRD9 gene analysis.

Exons	Primer designation	Primer sequence $(5' \rightarrow 3')$	Size (nt)	Ta (°C)	G/C%	Fragment size (bp)
1	Forward	TAGCTTCGAATCTGCCGCGCGA	22	60	59	500
	Reverse	TCTACCAGGAACGTAAGCGCCTA	23		52	
2	Forward	CATGCCGCCACTGTGGTCTTC	21	60	62	498
	Reverse	TACCAACGGAACACCCCCT	19		58	
3	Forward	GGCAGACCTGTCCGGATC	18	8 60 67	67	262
	Reverse	GTGCCGACCCCTCATTTACA	20		55	
4	Forward	ACTTAAAATGCTGTGAGACACCAGA	TAAAATGCTGTGAGACACCAGA 25 60	60	40	272
	Reverse	GGTCTGTTTCACAGCTGACGA	21		52	
5	Forward	CATGAACTCATTAGTGGCTCACTCT	25	60	44	526
	Reverse	CAGAAACACCTGTGAAAGCTCAA	23		44	
6	Forward	TCTTGGTAGTCATCTAGAGCTTTGC	25	60	44	274
	Reverse	GTTCACTGTGAGGCTCCCTT	20		55	
7	Forward	TGATTCTAGGAGCGGCTGTT	20	60	50	208
	Reverse	TGTGGTTTCCACAGAACCTTT	21		43	
8	Forward	CTCCAGGTGACTTGGTTGTCC	21	60	57	256
	Reverse	TGCTAGATCACACAGCACCAAC	22		50	
9	Forward	TGCTTTCACCCCCATTAAGCC	21	60	52	266
	Reverse	GCCATGGCTCAGCTTTTCATTAC	23		48	
10	Outer Forward	AATGAAAAGCTGAGCCATGGCCAT	24	64	46	1423
	Outer Reverse	TCCAACACGAGTTTCATTCCTG	22	64	45	
	Inner Forward	CCTGCACCAATCACATCCACT	21	60	52	284
	Inner Reverse	GCATTTGCCATCACTCCACTAA	22		46	
11	Forward	TTCCACACAGCTCTTTTGCTTGT 23 60	60	44	496	
	Reverse	GCACACATGTGGGACTCCACG	21		62	
12	Forward	GGCTCCTTTCAGCGTACCTT	20	60	55	226
	Reverse	GTCAGGCTGCAGGCTCTT	18		61	
13	Forward	AGCCATTTTTACGTGTGTGTAATGTC	26	60	39	262
	Reverse	ATCTTACTGATCAGAAACGGACTCCA	26		42	
14	Forward	AGTGATTTCAATAGCGAGTGTGAAGT	26	60	39	258
	Reverse	GGAGGCCGTGTGTTTTCTTC	20		55	
15	Forward	TAGGTCTTGTCTGATGCTTTGCT	23	60	44	497
	Reverse	AATGCTGCCCACTACCTCGTCTA	23		52	
16	Forward	AGGTCAGGAAGCAGACCTTG	20	60	55	218
	Reverse	AATAAAAGAGCTGAAGGTGGTCT	23		39	

Analyzer (Thermo Fisher Scientific).

2.7. Reverse transcription and quantitative real-time PCR (RT-qPCR)

RNA from A375 and WM115 cell variants, cDNA synthesis and relative quantitative Real-Time PCR was performed as described elsewhere [85] in a LightCycler 480 instrument (Roche). Primers are presented in Table 2.

2.8. Western blotting

Western blotting was performed to confirm the expression of BRD9 protein variants and study the effect of PROTAC BRD9 degrader-1 (HY-103632, MedChemExpress). A375 or WM115 cells were seeded in T-25 cm² flasks (6.5 \times 10⁵ cells/flask; 2.2 \times 10⁵ cells/mL), collected by scraping and lysed for 1 h using ice-cold radioimmunoprecipitation assay (RIPA) lysis buffer (89900, Thermo Fisher Scientific) with protease and phosphatase inhibitor mixture (PPC1010, Sigma Aldrich). For BRD9 depletion assays, cells were exposed to the 13.5 nM of PROTAC BRD9 degrader-1 according to the manufacturer's instructions, for 24 h. Protein concentration in cell extracts was determined using Pierce BCA protein assay kit (23225, Thermo Fisher Scientific). Cell lysates (25 μg) were resuspended in Laemmli buffer. The protein extracts were separated in a 10 % SDS-polyacrylamide gel electrophoresis and transferred onto methanol-activated polyvinylidene difluoride membranes (1620177, Bio-Rad) using the Trans-Blot® Turbo Blotting System (Bio-Rad). The membrane processing, immunoblot and development were performed as described elsewhere [86]. The primary antibodies used were anti-BRD9 (1:7500, ab137245, Abcam), anti-MPST (1:250, HPA001240, Sigma-Aldrich), anti-EAAT3 (1:1000, 14501S, Cell

Signaling Technology), anti α -tubulin clone B-5-1-2 (1:4000; T5168, Merck KGaA) and anti- β -actin (1,5000, A5441, Sigma Aldrich).

2.9. Proliferation assay

To study cellular proliferative rate, A375 or WM115 cells were plated in 24-well plates (5 \times 10^4 cells/well; 1 \times 10^5 cells/mL) in supplemented DMEM and left to adhere for 24 h in normal culture conditions. Cells were exposed or not to 0.402 mM L-cysteine (102839, Merck). At each time-point, cells were detached as described (cells suspended in medium were also collected) and centrifuged for 5 min at 155 \times g. Supernatant was discarded and total cells were counted, using a Neubauer improved cell counting chamber.

2.10. Wound healing assay

The migratory capacity of A375 or WM115 cells was evaluated using the wound healing assay. Cells were plated in 12-well plates (1 \times 10^5 cells/well/mL) until the formation of a confluent monolayer. Cells were exposed or not to 0.402 mM L-cysteine (102839, Merck). Once confluent, cells were incubated for 3 h with 5 µg/mL mitomycin-C (M4287, Sigma Aldrich) and a linear scratch in each monolayer was made with a 20 µL pipette tip, creating a wound across the well diameter. The media was replaced to remove debris and cells in suspension. Bright-field images of each well were acquired on the Olympus IX53 Inverted Microscope at each time-point. The wound closure was quantified using the ImageJ software (imagej.nih.gov/ij/).

Table 2Primers used in gene expression, *MPST* promoter constructs and relative occupancy quantification. Detailed characterization of the primers used in RT-qPCR assays, in pGL3-MPST promoter constructs and for chromatin immunoprecipitation (ChIP) assay.

Gene	Primer Primer sequence $(5' \rightarrow 3')$		Size	Ta	G/C	Fragment size
			(nt)	(°C)	%	(bp)
RT-gPCR						
Bromodomain-containing protein 9 (BRD9)	Forward	GCGACTTGAAGTCGGACGAGAT	22	62	55	128
	Reverse	GTCCACCACTTTCTTGCTGTAGC	23		52	
Cystathionine beta-synthase (CBS)	Forward	GAGCTCTTGGCCAAGTGTG	19	60	58	232
	Reverse	GCACGTCCACCTTCTCGG	18		67	
Cystathionine Gamma-Lyase (CTH)	Forward	GCAGCCACTGTAACTATTACCC	22 60 50		175	
	Reverse	CTGGTGTAATTGCTGCCTCTAG	22		50	
Mercaptopyruvate Sulfurtransferase (MPST)	Forward	CTTCATCAAGACCTACGAGGAC	22	60	50	134
	Reverse	GGTAGTGGCCAGGTTCAATG	20		55	
Glutamic-Oxaloacetic Transaminase 1 (GOT-1)	Forward	GAGAAGAGAGGATTGGACCTC	21	60	52	147
	Reverse	CATGACAGAAGCAATCTGCTTCC	23		48	
Glutamic-Oxaloacetic Transaminase 2 (GOT-2)	Forward	CCAGAGCCAGCTCCTGGT	18	61	67	171
, ,	Reverse	CTGCCTTGCGGACGCTAG	18		67	
Solute Carrier Family 7 Member 11 (SLC7A11)	Forward	GGTCCTGTCACTATTTGGAGC	21	61	58	136
	Reverse	GAGGAGTTCCACCCAGACTC	20		59	
Solute Carrier Family 1 Member 1 (SLC1A1)	Forward	GTATCACGGCCACATCTGCC	20	61	60	121
•	Reverse	GCAATGATCAGGGTGACATCC	21		52	
Hypoxanthine-guanine phosphoribosyltransferase	Forward	TGACACTGGCAAAACAATGCA	21	58	43	94
(HPRT1)	Reverse	GGTCCTTTTCACCAGCAAGCT	21		52	
pGL3-MPST promoter constructs						
MPST 5'UTR	Forward	ATC ACCCCTC ACCATCTTCCCC ACACTCC	29	67	52	
	Forward Mlu-I restriction	ATG <u>ACGCGT</u> CACCATGTTGGCCAGACTGG	29	0/	52	
(-870-28)	Miu-1 restriction Reverse	ATGAAGCTTGCGACAGGGAGGATGTCAG	29		48	
	Hind-III	ATGAAGGTTGCGACAGGGAGGATGTCAG	29		48	
	restriction					
ChIP assay						
MPST (a)	Forward	GCATACTCATGTGGGTAGGG	20	61	55	240
or (u)	Reverse	GAGGAAACTGAGGCTCAGAGG	20	01	57	270
MPST (b)	Forward	CTGCTCACACAGATGCTAGG	20	61	55	396
VII 01 (D)	Reverse	GCCACCCGGTGACATCCTAGG	18	01	72	390
SLC1A1	Forward	GCAAAACTACCGGGCTGG	18	60	61	202
HOIM	Reverse	GCAAAACTACCGGGCTGG	19	00	63	202
	VEAGISE	GUALIGIGGGIGGGIG	19		03	

2.11. Nuclear magnetic resonance analysis (¹H NMR)

Metabolic profiles were analyzed by $^1\mathrm{H}$ NMR. Briefly, cells were seeded in 175 cm 2 culture flasks (6,5 × 10 6 cells/flask; 5 × 10 5 cells/mL) and cultured in control conditions or exposed to 0.402 mM L-cysteine (102839, Merck). Cell extracts were treated and samples prepared as described [87]. The $^1\mathrm{H}$ NMR (noesypr1d) was obtained at 25 $^\circ\mathrm{C}$ in an Avance 500 II+ (Bruker) spectrometer operating at 500.133 MHz, equipped with a 5 mm TCI(F)-z H-C/N Prodigy cryo-probe. The chemical shifts in aqueous sample were referred to the TSP. Topspin 4.0.7 (Bruker) was used for acquisition and spectra analysis. Compound identification was performed by resorting to the Human Metabolome database (HMDB) and Chenomx NMR suite software version 8.1 (Chenomx Inc.). Metabolites' concentrations were determined using Chenomx NMR suite software version 8.1 for $^1\mathrm{H}$ NMR spectra (Chenomx Inc.).

2.12. Immunofluorescence

Cells were seeded in glass coverslips in 24-well plates coated with 0.2 % gelatin from porcine skin (G-1890, Sigma-Aldrich) (1 \times 10⁵ cells/ well: 2×10^5 cells/mL), and cultured as previously described. Once adherent, cells were fixed with 4 % paraformaldehyde for 15 min at 4 $^{\circ}$ C and permeabilized with 0.1 % saponin in PBS-BSA (0.5 %, w/v, BSA in PBS) for 15 min at room temperature. Immunofluorescence analysis was performed to determine the basal expression of MST and EAAT3 and to study the effect of PROTAC BRD9 degrader-1 (HY-103632, MedChemExpress). Fixed cells were then incubated overnight at 4 °C with anti-MPST (1:100, HPA001240, Sigma-Aldrich), anti-EAAT3 (1:100, 14501S, Cell Signaling Technology) and anti-BRD9 (1:100, ab137245, Abcam), and then incubated with secondary antibody for 2 h at room temperature (Alexa Fluor® 488 anti-rabbit, A-11034, Thermo Fisher Scientific). Slides were mounted in VECTASHIELD media with 4'-6diamidino-2-phenylindole (DAPI, H-1200-10, Vector Labs) and examined by standard fluorescence microscopy (Zeiss Imajer.Z1 AX10 microscope). Images were acquired and processed with CytoVision software (Leica Biosystems).

2.13. Promoter activity by luciferase reporter gene assay

A fragment of 5' UTR region (-870-28) of *MPST* gene were amplified by PCR (Table 2) and inserted in pGL3-Basic vector (E1751, Promega) using *Mlu*I and *Hind*III restriction sites and standard techniques [88]. Cells were transfected with 0.5 µg of each pGL3-*MPST* promoter construct, positive control (pGL3-Control; E1741; Promega) or negative control (pGL3-Basic), and co-transfected with 0.1 µg Renilla vector (E2810; Promega). Luciferase activity of constructs, Firefly and Renilla luciferases were measured using the Dual Luciferase Assay System (E1910, Promega) according to the manufacturer's protocol and results were acquired and analyzed as described [89].

2.14. H₂S quantification in cell homogenates

Cells were seeded in 6-well plates (5×10^5 cells/well, 2.5×10^5 cells/mL) and cultured in control conditions or exposed to 0.402 mM L-cysteine (102839, Merck) and/or 30 μ M NaHS (161527, Sigma-Aldrich) for 16 h. Then, cells were scraped in PBS and centrifuged at $210\times g$ for 5 min. The cell pellet was homogenized in NP40 lysis buffer (1% NP40, 150 mM NaCl, 50 mM Tris-Cl, pH 8.0) on ice for 30 min and centrifuged for 5 min at $20,000\times g$ 4 °C. Cell homogenates ($20~\mu$ L) were incubated in black 96-well plates with $10~\mu$ M 7-Azido-4-Methylcoumarin probe (AzMC, L511455, Sigma Aldrich) in the absence or presence of 1 mM o-(carboxymethyl)hydroxylamine hemihydrochloride (AOAA, C13408, Sigma Aldrich) and 3~mM DL-propargylglycine (PAG, P7888, Sigma Aldrich). H_2 S production was monitored following the fluorescent signal of AzMC probe (λ_{exc} : 355~nm; λ_{em} : 460~nm) every 30~min for 2~h, in a

VICTOR3 instrument from PerkinElmer/Wallac 1420 v3.0 software. The protein concentration of each lysate was determined with the Bradford method using protein assay dye reagent concentrate (500–0006, Bio-Rad). The $\rm H_2S$ production activities were normalized to the total protein concentration and to a blank sample (cellular lysates without probe).

2.15. ATP quantification

Cells were seeded in 6-well plates (5×10^5 cells/well, 2.5×10^5 cells/mL) and cultured in control conditions or exposed to 0.402 mM L-cysteine (102839, Merck) and/or $30~\mu$ M NaHS (161527 Sigma Aldrich) for 16~h. Then, cells were scraped in PBS containing 2~mM EDTA, centrifuged at $210~\chi g$ for 5~min and homogenized in 1~% NP40 lysis buffer (1~% NP40, 150~mM NaCl, 50~mM Tris-HCl, pH 8.0) with 5~% protease inhibitor (58830, Sigma) on ice for 30~min and centrifuged at $20,000~\chi g$ for 5~min at $4~^\circ C$. Protein concentration was quantified using the Bradford method. ATP determination kit (622066, Molecular probes) was used in accordance with the manufacturer's instructions, using an ATP calibration curve, within the $0-30~\mu M$ ATP range. The measurements were performed using the Luciferase protocol in a VICTOR3 (PerkinElmer), using the Wallac 1420~s of tware.

2.16. Chromatin immunoprecipitation (ChIP) analysis

To analyze potential interactions between the transcription factor NRF2 and ARE sequences in *MPST and SLC1A1* promoters, ChIP was employed. We identified two putative ARE sequences recognized by NRF2 in the *MPST* promoter and one in the *SCL1A1* promoter, and designed primers for those regions to perform ChIP analysis. Cell preparation and ChIP assay were performed using the OneDay ChIP kit (kchonedIP-060, Diagenode) according to the manufacturer's protocol. The chromatin complexes were immunoprecipitated with 1 μ g/mL of specific anti-human NRF2 antibody (ab31163; Abcam). The relative occupancy of the immunoprecipitated factors at a specific promoter region was performed by absolute qPCR, using primers for *MPST* and *SLC1A1* promoter (Table 2) and calculated using the following formula:

 $Relative \ occupancy = 2^{(CtNegCtl-CtTarget)}$

2.17. Melanin quantification

Melanin content was measured through spectrophotometry as described elsewhere [90]. Cells were exposed or not to 0.402 mM L-cysteine (102839, Merck) for 16 h after 16 h of starvation. Briefly, A375 and WM115 cell variants were collected with no phenol red 2.5 % Trypsin $10\times$ (15090046, Thermo Fisher Scientific) as described previously, and counted using a Neubauer improved cell counting chamber. Cells were resuspended in 1 M NaOH and the melanin content was measured at 490 nm. Melanin concentration was determined through a standard curve (0 to 200 $\mu g/mL$ range) obtained with synthetic melanin (M0418, Sigma Aldrich).

2.18. Metabolic viability assays

All variants of A375 and WM115 were plated in 96-well clear plates (2 \times 10^4 cells/well; 2 \times 10^5 cells/mL) and treated with a commercial MST inhibitor (I3MT-3, HY-128206, CAS No.459420-09-8, MedChemExpress) at increasing concentrations (0, 30 μM , 100 μM , 300 μM , 600 μM and 900 μM). Upon 48 h of exposure, metabolic viability assays were performed by colorimetry using Cell Proliferation Reagent WST-1 (11644807001, Roche), according to the manufacturer's instructions.

2.19. Cell death assays

All variants of A375 and WM115 were seeded in 24-well plates (1 imes

 10^5 cells/well; 2 \times 105 cells/mL). After exposure to MST inhibitor (I3MT-3, HY-128206, CAS No. 459420-09-8, MedChemExpress), cells were collected and labeling with FITC-labeled Annexin V (640906, BioLegend) and propidium iodide (PI; P4170, Sigma Aldrich Aldrich) was performed as described [86]. Results were analyzed by flow cytometry (BD FACSCanto II). FlowJo X v10.0.7 software (https://www.flowjo.com/) was used to analyze data.

2.20. Three-dimensional (3D) in vitro melanoma skin model

To establish the three-dimensional melanoma skin model used, we adapted the protocols published elsewhere [91,92]. Essentially, porous polystyrene scaffolds (Alvetex®, AVP005-48, REPROCELL Europe Ltd.) with an area of 1.13 cm² were inserted in 6-well plates and pretreated with 70 % ethanol for 30 min to render them hydrophilic properties. The scaffolds were washed twice with phosphate-buffered saline (PBS) and 2 \times 10⁶ HDFns were seeded onto the scaffolds in 100 µL of HDFn medium, followed by incubation in a humidified incubator at 37 °C with 5 % CO₂ for 1.5 h to allow cell adhesion. Next, the scaffolds containing HDFns were submerged with 9 mL of HDFn medium supplemented with 100 µg/mL L-ascorbic acid (11487487, Fisher Scientific) and maintained up to a further 15 days at 37 °C in a 5 % CO2 humidified incubator. The culture medium was renewed every 5 days to allow the formation of a dermal equivalent. After this, 5×10^4 A375 or 1×10^5 WM115 melanoma cells were seeded on the dermis equivalents in 2 mL of melanoma culture medium supplemented or not with 0,402 mM L-cysteine (102839, Merck). After incubating for 3 days at 37 °C and 5 % CO₂, 1 \times 10⁶ HEKns were added in 2 mL of HEKn medium containing the final concentration of 1.5 mM calcium chloride (Gibco) without L-cysteine (102839, Merck). Finally, after further 3 days of incubation, keratinocytes were exposed to air-liquid interface and the culture medium was changed to HEKn medium containing the final concentration of 1.5 mM calcium chloride (Gibco), 10 ng/uL keratinocyte growth factor (K1757, Sigma), 50 µg/mL L-ascorbic acid (11487487, Fisher Scientific) and 0,402 mM L-cysteine (102839, Merck) or not. The medium was changed every 2 days for 18 days to allow HEKn differentiation in the several epidermis strata, as well as melanoma cell invasion into the dermis. The tissues were fixed overnight in 10 % neutral buffered formalin (Formalin 10 %, Cat. number 9713.9010, VWR) and embedded in paraffin. Sections (4 um) were stained with hematoxylin and Eosin staining (H&E, Hematoxylin, Cat. Number CS700, Dako; and Eosin, Cat. Number CS701, Dako). Melanoma thickness was measured in 20 different spots in two biological replicates using Aperio ImageScope software (https:// www.leicabiosystems.com/en-pt/digital-pathology/manage/aperio-im agescope/).

2.21. Immunohistochemistry

The invasion of melanoma cells, in 3D skin model, was evaluated upon immunodetection of S-100 protein, which is expressed in neural crest-derived cells, being considered an efficient melanoma marker [93,94]. Immunohistochemistry analysis was performed using anti–S100 (Cat. Number 760-2523, Roche Diagnostics, pre-diluted for 16 min; pretreatment CC1–48 min; Ventana Medical Systems) with appropriate positive and negative controls samples, on the BenchMark ULTRA IHC/ISH Automatic staining platform (Ventana Medical Systems) using OptiView DAB IHC Detection Kit with diaminobenzidine as the chromogen to detect antigen expression. Tissue sections were counterstained with Mayer's hematoxylin before mounting.

2.22. Statistical analysis

Statistical analyses and half maximal inhibitory concentration (EC $_{50}$) values were performed in GraphPad Prism 8.0 software (www.graphpad.com). Data are presented as mean \pm SD. Assays were performed with at least three biological replicates. For comparisons of two groups, a

two-tailed unpaired t-test was used. For more than two groups, one-way and two-way analyses of variance (ANOVA) were used. Statistical significance was established as p < 0.05.

3. Results

3.1. Analysis of BRD9 mutational profile in a cohort of familial CM patients predicts identified BRD9 SNVs as benign

BRD9 physiological functions and role in CM are not completely understood. In order to further disclose the function of altered BRD9 in hereditary CM, we evaluated the BRD9 mutational profile in a cohort of familial CM patients (n = 72) from IPOLFG, by Sanger sequencing, to investigate the presence of variants in both coding and non-coding regions. Overall, we identified 21 BRD9 single nucleotide variants (SNVs), including 2 in 5UTR, 13 intronic SNVs and 6 exonic SNVs (Table 3). However, most of them were considered common polymorphisms in the European population, presenting an allele frequency >1 % according to gnomAD genomes r3.0 and 1000 Genomes databases [95,96]. Eight BRD9 rare SNVs in the European population were identified by Sanger sequencing: c.-65G>A, 1.4 % (1/72) in 5'UTR; c.1043-19C>T, 1.4 % (1/ 72), c.1383 + 37C>G, 1.4 % (1/72), and c.1383 + 29G>A, 9.7 % (7/72) intronic variants; c.6C>G, 5.6 % (4/72), c.183G>C, 5.6 % (4/72), c.816G>A, 4.2 % (3/72) and c.1190T>C, 1.4 % (1/72) exonic variants (highlighted in blue in Table 3). Out of 72 patients, 16 were identified with at least one rare variant in BRD9. All these 16 familial CM patients, 8 indexes with familial CM and 8 MPM cases, were negative for pathogenic germline mutations in the current criteria genes for hereditary melanoma (CDKN2A, CDK4 and MITF (c.952G> A/p.E318K)). Among the rare exonic SNVs, c.183G>C and c.1190T>C are missense variants, leading to single amino acid changes, while the other ones are synonymous (c.6C>G, c.816G>A) (Table 3). Overall, BRD9 c.183G>C was identified in 5.6 % of this cohort (Table 3). Only 4 patients showed two or more BRD9 rare variants, 2 of them were selected for whole exome sequencing (WES) study performed by us [21]. Interestingly, the same BRD9 mutational profile was found in 2 patients, which includes the exonic variants c.183G>C (missense) and c.816G>A (synonymous) but also c.1383+29G>A, located in intron 13.

None of the identified *BRD9* SNVs have their clinical significance reported according to the ClinVar database, except c.816G>A (rs74984870), described as benign. It is important to highlight that c.74G>A and c.-65G>A *BRD9* 5'UTR variants were both found in homozygosity (the first in only one patient, Table 3), which is not consistent with the autosomal dominant inheritance pattern characteristic of CM susceptibility [21].

Given the well-documented impact of pathogenic SNVs on gene expression (at transcriptional and post-transcriptional levels) and protein function, but also their potential role in cancer susceptibility, we decided to analyze the effect of BRD9 rare SNVs at distinct levels of gene function, using predictive in silico tools (Fig. 1). Since the set of BRD9 rare SNVs includes coding and non-coding variants, the predictive programs were selected according not only to the effect of amino acid substitution on protein function, structure, and stability, but also according to regulatory changes and impact on splicing. We only considered an overall pathogenic variant when most available in silico tools suggested a deleterious effect. Thus, all BRD9 rare SNVs were considered likely benign according to the selected predictors and the mentioned criteria (Fig. 1). In addition, we sought to understand the potential effect of the missense mutations by analyzing the corresponding amino acid substitutions in the structural model of BRD9 obtained from Alphafold. However, both substitutions are located in regions of the protein for which the model cannot reliably assign elements of secondary structure. Therefore, the structural and functional impact of these substitutions at the protein level remains undetermined.

Table 3 List of 5'UTR, intronic and exonic SNVs found by Sanger sequencing in the IPOLFG cohort of familial cutaneous melanoma (CM) patients (n=72). The rare variants, presenting a European population frequency <1 %, are highlighted in blue. Nucleotide change according to dbSNP HGVS (GRCh38.p13 chromosome 5, *BRD9* transcript variant 1, NM_023924.5). Their dbSNP reference (rs) number, genome location, gene location, amino acid change (when applicable), type (molecular consequence) and frequency (%) in IPOLFG cohort of familial CM patients are also presented.

dbSNP reference (rs) number	Genome location (5p15.33)	Gene location	Nucleotide change	Amino acid change	Type	Frequency in CM (%)	European population frequency (%)*
rs111286164	892731	5'UTR region	c74G>A		5UTR	2.8 (2/72)	5.0
rs542129307	892722	5'UTR region	c65G>A	-	5UTR	1.4 (1/72)	0.04
rs72703159	889579	Intron 5	c.461 + 8G > T	-	Splice region variant	6.9 (5/72)	4.7
rs72703154	889212	Intron 5	c.462-47C>T	_	Intronic	6.9 (5/72)	3.2
rs72703155	889254	Intron 5	c.462-89G>A	_	Intronic	2.8 (2/72)	5.0
rs66859331	889382	Intron 5	c.461+205G>T	_	Intronic	2.8 (2/72)	5.0
rs10062549	889281	Intron 5	c.462-116C>T	_	Intronic	8.3 (6/72)	5.1
rs546947145	879908	Intron 10	c.1043-19C>T	_	Intronic	1.4 (1/72)	0.05
rs41283151	878632	Intron 11	c.1139-145T>C	_	Intronic	8.3 (6/72)	40.4
rs41283153	878645	Intron 11	c.1139-158G>T	_	Intronic	2.8 (2/72)	4.7
rs184819406	876064	Intron 13	c.1383+37C>G	_	Intronic	1.4 (1/72)	0.4
rs72703144	876046	Intron 13	c.1383+55C>T	_	Intronic	9.7 (7/72)	6.2
rs10039297	876072	Intron 13	c.1383+29G>A	_	Intronic	9.7 (7/72)	0.2
rs55744146	871483	Intron 14	c.1422+43T>C	_	Intronic	8.3 (6/72)	5.3
rs28497180	870440	Intron 14	c.1525+33T>C	_	Intronic	5.6 (4/72)	5.3
rs375328319	892652	Exon 1	c.6C>G	p.G2=	Synonymous	5.6 (4/72)	0.9
rs199607133	891724	Exon 2	c.183G>C	p.E61D	Missense	5.6 (4/72)	0.03
rs141678469	891195	Exon 3	c.360G>A	p.P120=	Synonymous	1.4 (1/72)	1.8
rs74984870	886609	Exon 7	c.816G>A	p.P272=	Synonymous	4.2 (3/72)	0.04
rs145107515	878436	Exon 11	c.1190T>C	p.V397A	Missense	1.4 (1/72)	0.4
rs1051630	870504	Exon 14	c.1494T>C	p.V498=	Synonymous	8.3 (6/72)	5.3

3.2. Overexpression of BRD9 and BRD9 c.183G>C induces a less proliferative but more migratory phenotype in A375 CM cells

Given that the c.183G>C SNV had been already identified in a smaller Portuguese cohort [21], we hypothesized that, although it was predicted to have benign effects by in silico analysis (Fig. 1), this variant could induce alterations in CM cells that could correlate with hereditary CM features. To test this hypothesis, we transfected A375 melanoma cells with a BRD9-encoding plasmid (A375 BRD9 WT), as well as BRD9 (c.183G>C)-encoding plasmid. In addition, we transfected the empty pCMV6 vector as a negative control. We then obtained A375 clones successfully overexpressing wild-type (WT) or c.183G>C BRD9 at mRNA and protein levels (Fig. 2A, B and C). To disclose the cellular effects of both BRD9 forms in A375 cells, we studied the proliferation rate of these clones over 48 h and found that both A375 BRD9 WT or BRD9 c.183 G>C showed a significant reduction in proliferation from 6 h, and substantial reduction of proliferative capacity at 48 h, when comparing to control even in the presence of cysteine (Fig. 2D and E). We then wondered if these BRD9 alterations could also affect the migratory capacity of these cells. We assessed cell migration by wound healing over a period of 48 h, in the presence of mitomycin to exclude the interference of cell proliferation on the wound closure. Interestingly, we found that both A375 BRD9 WT or BRD9 c.183 G>C showed a significant increase in migration capacity, when comparing with control, starting at 10 h, in the absence and presence of cysteine (Fig. 2F and G). We can, then, conclude that overexpression of BRD9 in its WT or c.183G>C variants promotes a shift in cellular features, inducing a less proliferative but more migratory phenotype in A375 cells.

3.3. BRD9 wild-type and BRD9 c.183G>C overexpression induces metabolic remodeling in A375 CM cells

Alterations in cellular features induced by overexpression of *BRD9* and *BRD9* c.183G>C in this cell line, led us to wonder if A375 altered phenotype could be due to metabolic shifts induced by these genetic alterations.

¹H NMR analysis showed that several amino acids show contrasting

trends, when comparing to control (A375 empty) levels (Fig. 2H). Glutamate tended to decrease in A375 BRD9 WT and A375 BRD9 c.183G>C. The same tendency was observed for glycine, which presents more prominently in A375 BRD9 c.183G>C than in A375 BRD9 WT. Glutamine levels appear to be low and are only noteworthy in A375 BRD9 c.183G>C. Interestingly, methionine levels seemed to decrease only in A375 BRD9 c.183G>C, which indicates that a downstream rewiring in cysteine production may be occurring. While cysteine was not detected in the analysis of any cell variants, the levels of reduced glutathione (GSH) were similar between them, which may indicate that cysteine is being rapidly consumed to maintain glutathione availability, since it is a rate-limiting amino acid for glutathione synthesis (Fig. 2H). Moreover, we also found different metabolic patterns concerning sugar and organic acids metabolism (Fig. 2I and J), as for acetate and choline, which seem to increase in A375 BRD9 c.183G>C, and creatine, which decreases in A375 BRD9 WT (Fig. 2I and J). Notably, upon cysteine exposure, all A375 cell variants presented a trend to decrease the availability of glutamate and glycine. Accordingly, the GSH levels also tended to decrease upon cysteine exposure in A375 cells overexpressing WT or mutated BRD9, which indicates that this metabolic remodeling may require GSH consumption in order to keep the metabolic rate upon accelerating glutathione turnover. Moreover, cysteine canalization as a supplier for other pathways can also be an explanation, since cysteine catabolism dependent on MST seem to be active. Cysteine exposure further induced alterations in sugar and organic acids levels, as well as in other relevant metabolites, as creatine and creatine phosphate (Figs. 3A, B and C). Metabolic profiling led to the conclusion that both A375 BRD9 WT and A375 BRD9 c.183G>C present metabolic variations.

3.4. BRD9 wild-type and BRD9 c.183G>C overexpression modulates cysteine metabolism in A375 CM cells

The impact of *BRD9* WT and *BRD9* c.183G>C overexpression on the modulation of cysteine synthesis and reductive degradation in A375 cells, was assessed by the quantification of mRNA expression of key enzymes and transporters, namely: CBS (*CBS* gene), CSE (*CTH* gene), MST (*MPST* gene), cytosolic CAT (*GOT-1* gene), mitochondrial CAT

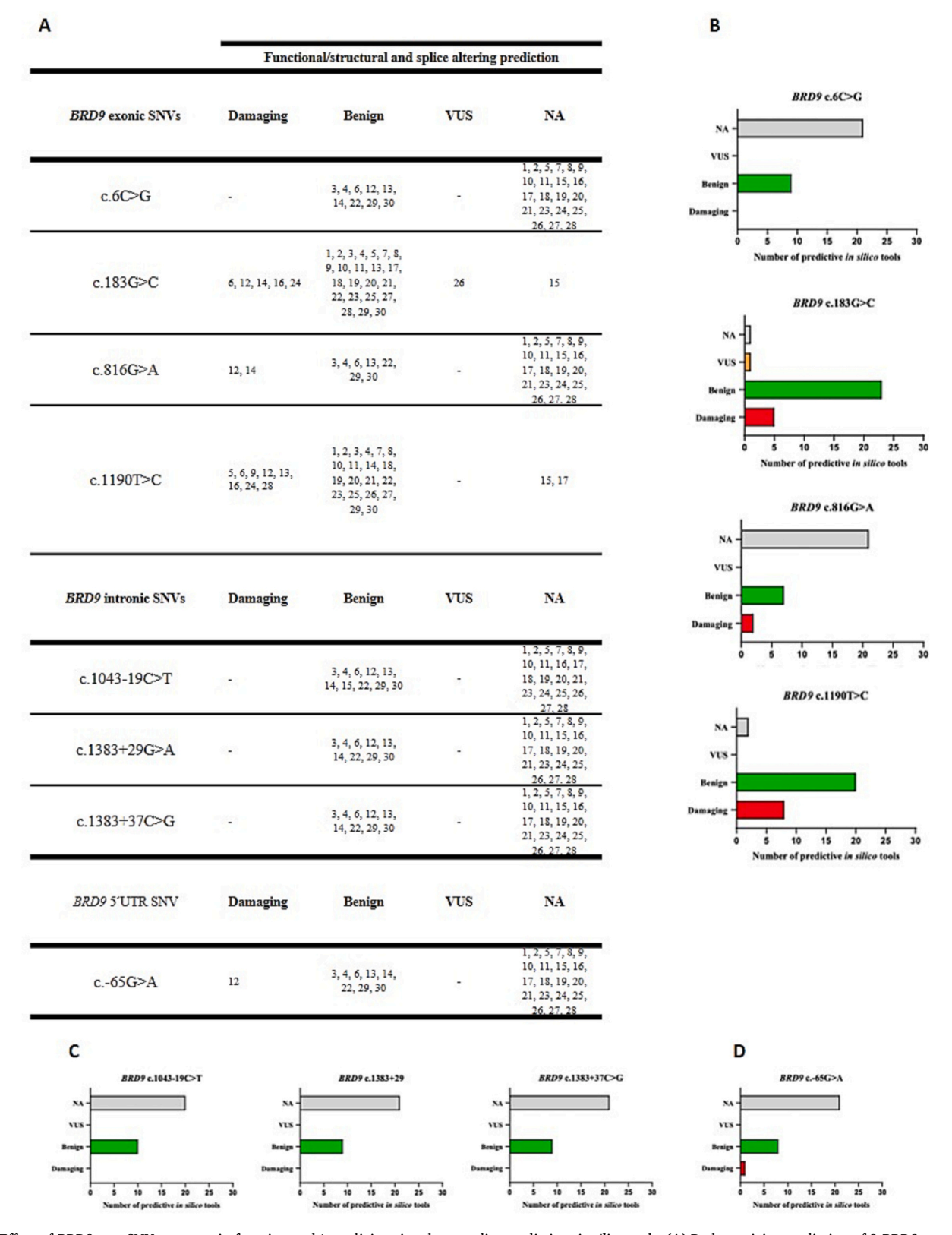
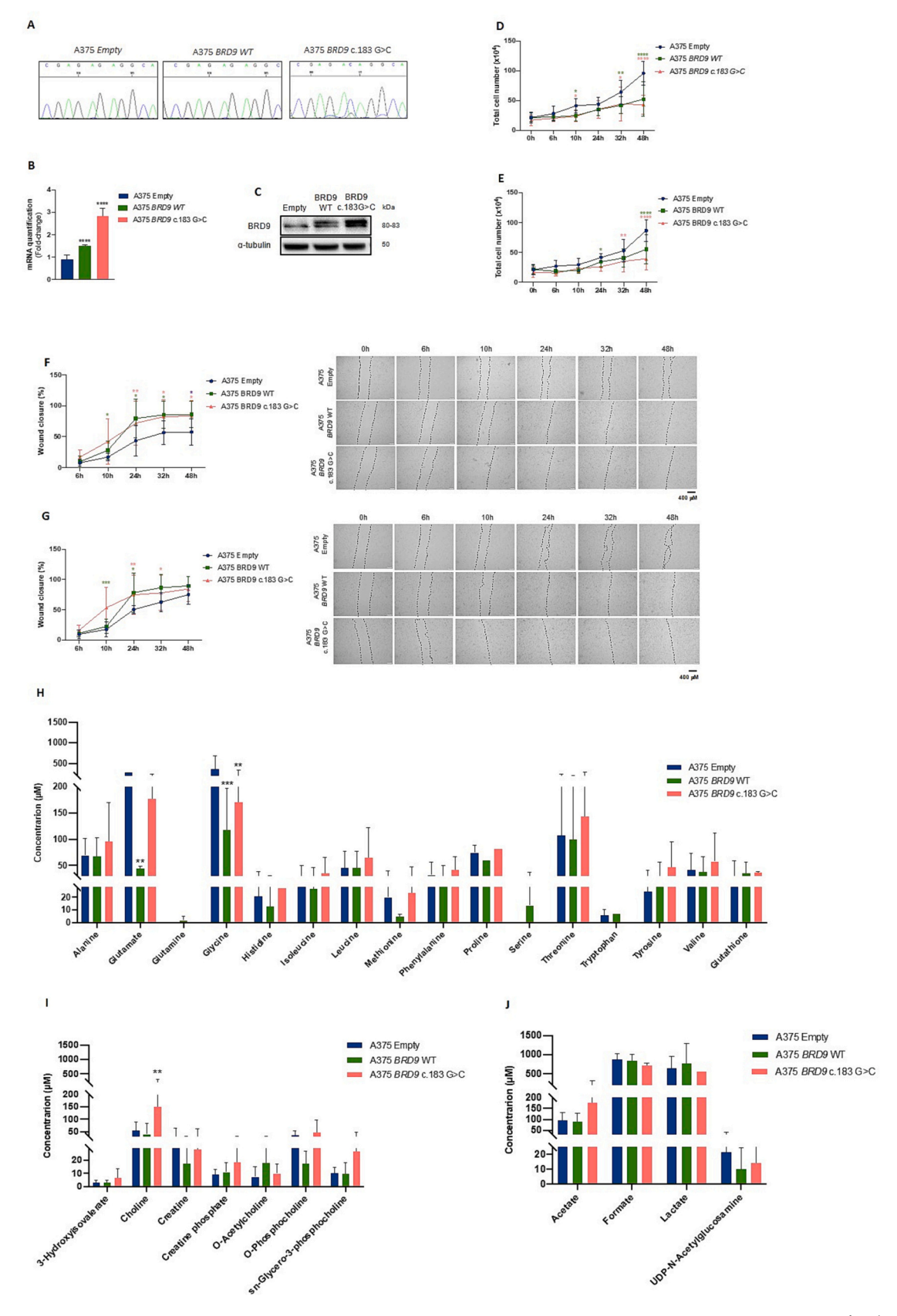


Fig. 1. Effect of *BRD9* rare SNVs on protein function and/or splicing signals according to distinct *in silico* tools. (A) Pathogenicity prediction of 8 *BRD9* rare SNVs (4 exonic, 3 intronic and 1 in 5UTR) according to 30 *in silico* bioinformatic tools. Predictive programs: 1, BayesDel_addAF; 2, BayesDel_noAF; 3, CADD; 4, Cancer Genome Interpreter; 5, Condel; 6, DANN; 7, DEOGEN2; 8, EIGEN; 9, EIGEN-PC; 10, FATHMM cancer (coding SNVs); 11, FATHMM inherited disease (coding SNVs); 12, FATHMM-MKL; 13, FATHMM-XF; 14, Human splicing finder; 15, IntSplice2; 16, LIST-S2; 17, M-CAP; 18, MetaLR; 19, MetaRNN; 20, MetaSVM; 21, Mutation Assessor; 22, MutationTaster2021; 23, MVP; 24, Polyphen-2; 25, PROVEAN; 26, PrimateAl; 27, REVEL; 28, SIFT; 29, SpliceAl; 30, TraP. The number of *in silico* tools out of the total available used for each variant analysis is represented in brackets. (B-D) Simplified output representation of pathogenicity predictive programs for (B) panel of *BRD9* rare exonic SNVs (C) panel of *BRD9* rare intronic SNVs and (D) 5UTR *BRD9* rare SNV. Graphic representation refers to the number of *in silico* tools corresponding to each predictive category (Damaging (red), Benign (green), VUS (orange) and NA (grey)). NA, not available; UTR, Untranslated region; VUS, Variant of unknown significance.



(caption on next page)

Fig. 2. BRD9 wild-type and BRD9 c. 183G>C overexpression induces a less proliferative but more migratory phenotype and rewires amino acid metabolism in A375 melanoma cells. By Sanger sequencing the sequence mRNA was confirmed (A) and by qPCR (B) and western blotting (C) the transfection of A375 melanoma cells and the expression of the BRD9 variants was confirmed. A375 cells transfection with wild-type overexpression and BRD9 c. 183G>C (over)expression vectors induced increased mRNA and protein levels of BRD9, comparing to empty vector. Overexpression of BRD9 WT or BRD9 c. 183 G>C induced a decreased proliferation rate in A375 cells, comparing to empty vector, in the absence (D) and presence (E) of cysteine. (F) Overexpression of BRD9 WT or BRD9 c. 183 G>C induced an increased migration capacity in A375 cells, by wound healing, comparing to empty vector, in the absence of cysteine. (G) Overexpression of BRD9 WT or BRD9 c. 183 G>C induced an increased migration capacity in A375 cells, by wound healing, comparing to empty vector, in the presence of cysteine. (H-J) Nuclear magnetic resonance spectroscopy of transfected A375 melanoma cells extracts in the absence of cysteine indicates that BRD9 WT and BRD9 c. 183 G>C overexpression induces a metabolic remodeling in several key metabolic pathways. Data is represented as mean \pm SD. *p < 0.5, **p < 0.01, ****p < 0.001, ****p < 0.0001. Experiments were performed with biological triplicates.

(GOT-2 gene), xCT (SLC7A11), and EAAT3 (SLC1A1). Interestingly, the overexpression of BRD9 WT strongly repressed the expression of the entire panel of studied genes, comparing to control. Moreover, overexpression of c.183G>C BRD9 exhibited a similarly repressive, yet highly attenuated, pattern regarding CBS, CTH, GOT-1, GOT-2 and SLC7A11 expression. Surprisingly, A375 BRD9 c.183G>C appeared to induce MPST and SLC1A1 expression, comparing to control (Fig. 3D and E). These results were confirmed at the protein level (MST and EAAT3, Fig. 3F and G). To confirm the differential effect of BRD9 WT and mutated variants on MPST expression, we exposed A375 empty, BRD9 WT and BRD9 c.183 G>C to BRD9 degrader-1 and analyzed the expression of BRD9 and MST proteins. Our results indicate that PROTAC BRD9 degrader-1 depleted BRD9 WT but not mutated BRD9 (Fig. 3H and J). Therefore, the effect of BRD9 WT on MST expression was abrogated but mutated BRD9 still upregulated the expression of MST (Fig. 3I and K), as previously observed. These results indicate that BRD9 degrader-1 does not deplete the mutated variant.

We then studied the effect of these expression shifts in cysteine related enzymes and transporters on the production of H₂S, which, as stated above, is produced through cysteine reductive degradation by CBS, CSE and/or CAT/MST. In these assays, we analyzed H₂S levels in the absence or presence of AOAA and PAG, inhibitors of the reverse transulfuration enzymes CBS and CSE, to estimate their relative roles with respect to MST (or other H₂S sources). A375 cells overexpressing either *BRD9* WT or *BRD9* c.183G>C presented an increase in H₂S levels, which were not altered by CBS/CSE inhibitors (Fig. 4A). While the increase in H₂S levels in *BRD9* c.183G>C-overexpressing cells matched the increase in MST expression, the same correlation was not observed with *BRD9* WT-overexpressing cells (Fig. 4A). It cannot be excluded that the capacity of cells to disposing of H₂S may have also been affected.

Pre-incubation of the cells with cysteine did not induce any change in steady-state $\rm H_2S$ levels between the three cell lines. Moreover, cysteine seems to have abrogated the *BRD9*-induced increase in $\rm H_2S$ levels, as compared to the control conditions (Fig. 4A). Pre-incubation with the polysulfides-containing $\rm H_2S$ donor NaHS increased $\rm H_2S$ levels in every cell line, irrespectively of co-incubation with cysteine, in the absence of inhibitors (Fig. 4A). The extent of $\rm H_2S$ levels decrease in the presence of AOAA+PAG was more evident in NaHS-incubated cells.

Since H₂S can serve as a source of electron equivalents to the mETC, we checked the effect of *BRD9* overexpression on the ATP levels. In control conditions, overexpression of *BRD9* WT or c.183G>C did not significantly change ATP levels. Incubation with NaHS in the absence or presence of cysteine resulted in a mild increase in ATP levels in all cell lines, whereas co-incubation with cysteine alone showed no significant effect comparing to control (Fig. 4B). In the presence of AOAA+PAG, in comparison with control cells bearing the empty vector and with control conditions, ATP levels were significantly lower for *BRD9* c.183G>C expressing A375 cells pre-incubated with cysteine and for cells expressing either *BRD9* variant pre-incubated with cysteine (Fig. 4B).

3.5. BRD9 status modulates MPST but not SLC1A1 through NRF2, inducing a remodeling in the melanin production pathway

Since BRD9 can modulate the action of NRF2, which is described to modulate SLC1A1 expression [69], and MST is an H_2S -producing AOE,

we hypothesized that NRF2 regulates not only *SLC1A1* but also *MPST* expression. ChIP analysis revealed that NRF2 does not seem to bind to *SLC1A1* promoter not even in the presence of cysteine nor among the different variants of *BRD9* expressed in A375. We found, however, that NRF2 binding to *MPST* promoter in A375 *BRD9* c.183 G>C is increased and stimulated by cysteine (Fig. 4C). Luciferase activity studies of *MPST* promoter in all A375 cell variants were performed, in the presence or absence of cysteine. Our results indicate that cysteine significantly decreased *MPST* promoter activity in A375 *BRD9* WT cells (Fig. 4D). No significant changes were seen in A375 empty nor in A375 *BRD9* c.183 G>C (Fig. 4D).

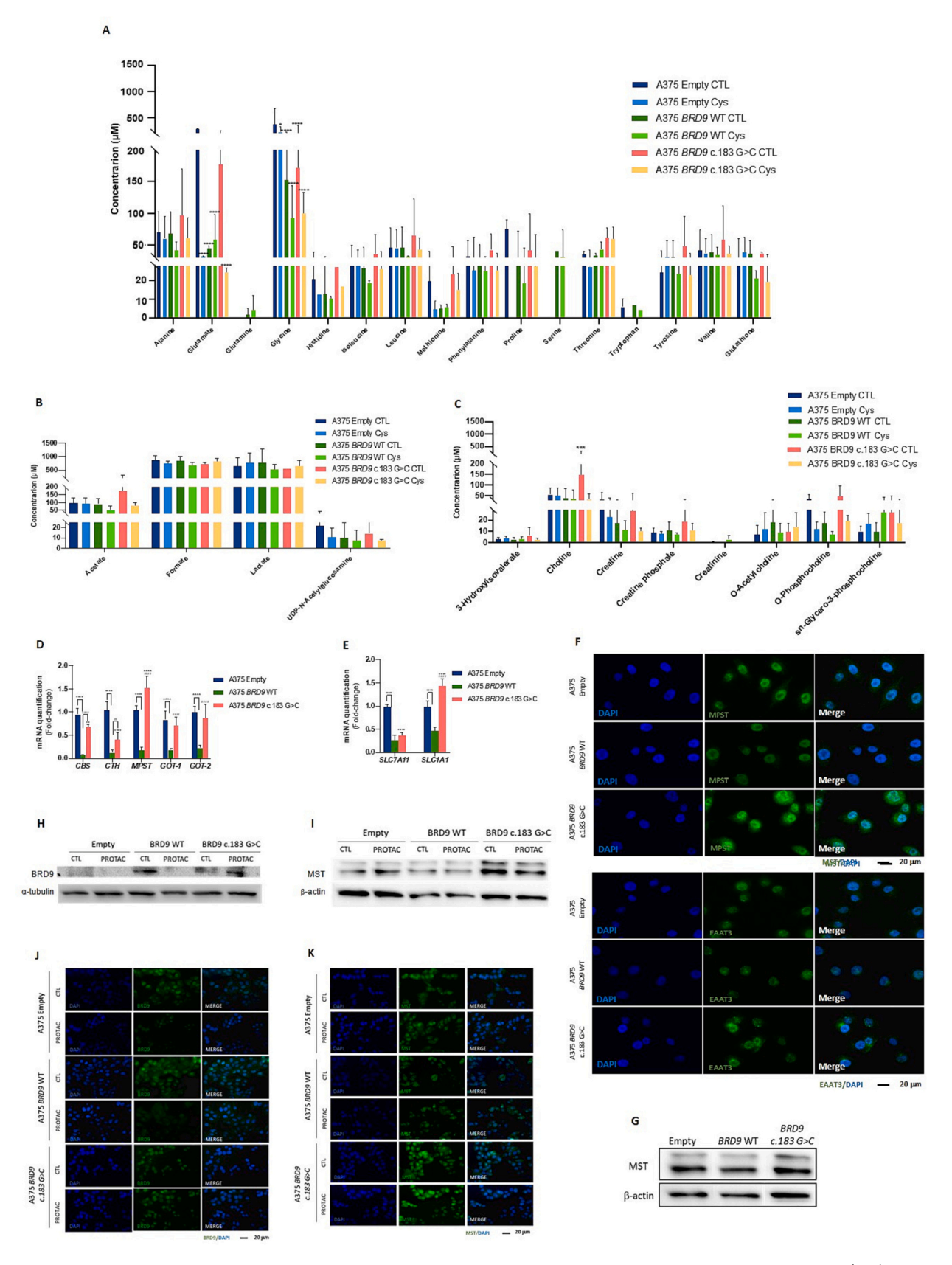
We further evaluated the effect of overexpressing WT or c.183 G>C BRD9 in A375 melanin production. In control culture conditions, A375 BRD9 WT presented the lowest level of melanin production, while cysteine prompted the decrease of melanin levels in A375 BRD9 c.183G>C (Fig. 4E and F).

3.6. BRD9 wild-type and BRD9 c.183G>C overexpression in WM115 cell line does not modulate MPST/MST and SLC1A1/EAAT3 expression

To study if our results could be replicated in another melanoma cell line and if BRD9 status was the only factor inducing these metabolic and expression alterations, we chose to transfect WM115 cells with the BRD9-encoding plasmids. We then successfully obtained WM115 clones overexpressing BRD9 WT or BRD9 c.183G>C (Fig. 5A). This was confirmed at mRNA (Fig. 5B) and protein levels (Fig. 5C). We then studied the expression of both MPST and SLC1A1 in the transfected WM115 control, WM115 BRD9 WT or WM115 BRD9 c.183G>C variants. WM115 BRD9 WT presented decreased MPST and SLC1A1 mRNA, comparing to WM115 transfected with the empty vector. However, WM115 BRD9 c.183G>C also showed a significant decrease in MPST and SLC1A1 expression, comparing to control (Fig. 5D). The same trend was found in protein expression of both MST and EAAT3 (Fig. 5E and F). Notably, the WM115 cell line expresses high basal levels of MPST/MST and SLC1A1/EAAT3, but no alteration was seen concerning the effect of BRD9 variants. WM115 BRD9 WT or WM115 BRD9 c.183G>C did not present significant differences in cell migration capacity in the absence or presence of cysteine (Fig. 5G and H). We also analyzed melanin production in these variants, and found that, although no differences were found in the absence of cysteine, in the presence of cysteine, WM115 BRD9 c.183G>C significantly increased melanin production (Fig. 5I and J). Moreover, ChIP analysis showed no binding of NRF2 to SLC1A1 or MPST promoters (Fig. 5K).

3.7. BRD9 c.183 G>C increases invasiveness of A375 CM cell line in a 3D in vitro skin model

To address the role of *BRD9* (WT and c.183 G>C) in melanoma aggressiveness, the capacity of invasion of A375 and WM115 cell line variants was tested in a 3D *in vitro* skin model. As observed in Fig. 6A and B, a higher invasive capacity of A375 cells, comparing to WM115 cells, was verified, since WM115, although presenting primary tumors, does not invade. However, upon cysteine exposure, WM115 control and *BRD9* WT formed statistically significant thicker tumors than in the absence of cysteine. Considering the A375 variants, the exposure to



(caption on next page)

Fig. 3. BRD9 wild-type and BRD9 c.183G>C overexpression alters the metabolic response of A375 cells to cysteine availability and modulates cysteine metabolic enzymes and transporters mRNA and protein expression. (A-C) Nuclear magnetic resonance spectroscopy of transfected A375 melanoma cells extracts in the presence (Cys) or absence (CTL) of cysteine indicates that BRD9 wild-type and BRD9 c.183G>C overexpression modulates the metabolic response to cysteine exposure, regarding intracellular amino acid, sugars and organic acids metabolism and other metabolic compounds. (D) By qPCR, mRNA levels of genes encoding enzymes CBS, CTH, MPST, GOT-1 and GOT-2, as well as (E) genes encoding cyst(e) ine transporters SLC7A11 and SLC1A1 in A375 transfected cells were quantified and it was observed that induction of BRD9 WT and c.183G>C variants overexpression regulates the expression of cysteine enzymes and transporters. A375 BRD9 c.183 G>C induces an upregulation of both MPST and SLC1A1, analyzed by qPCR. (F) Protein expression of MST and EAAT3 show upregulation of both proteins induced by BRD9 c.183 G>C induction, evaluated by immunofluorescence for MSt and EAAT3, and (G) western blotting for MST. Western blotting of BRD9 (H) and MST (I) in A375 cells exposed to PROTAC BRD9 degrader-1. Immunofluorescense to BRD9 (J) and MST (K) in A375 cells exposed to PROTAC BRD9 degrader-1. Data is represented as mean \pm SD. *p < 0.5, **p < 0.01, ****p < 0.001, ****p < 0.0001 (* in relation to Empty; # in relation to BRD9 WT). Experiments were performed with biological triplicates.

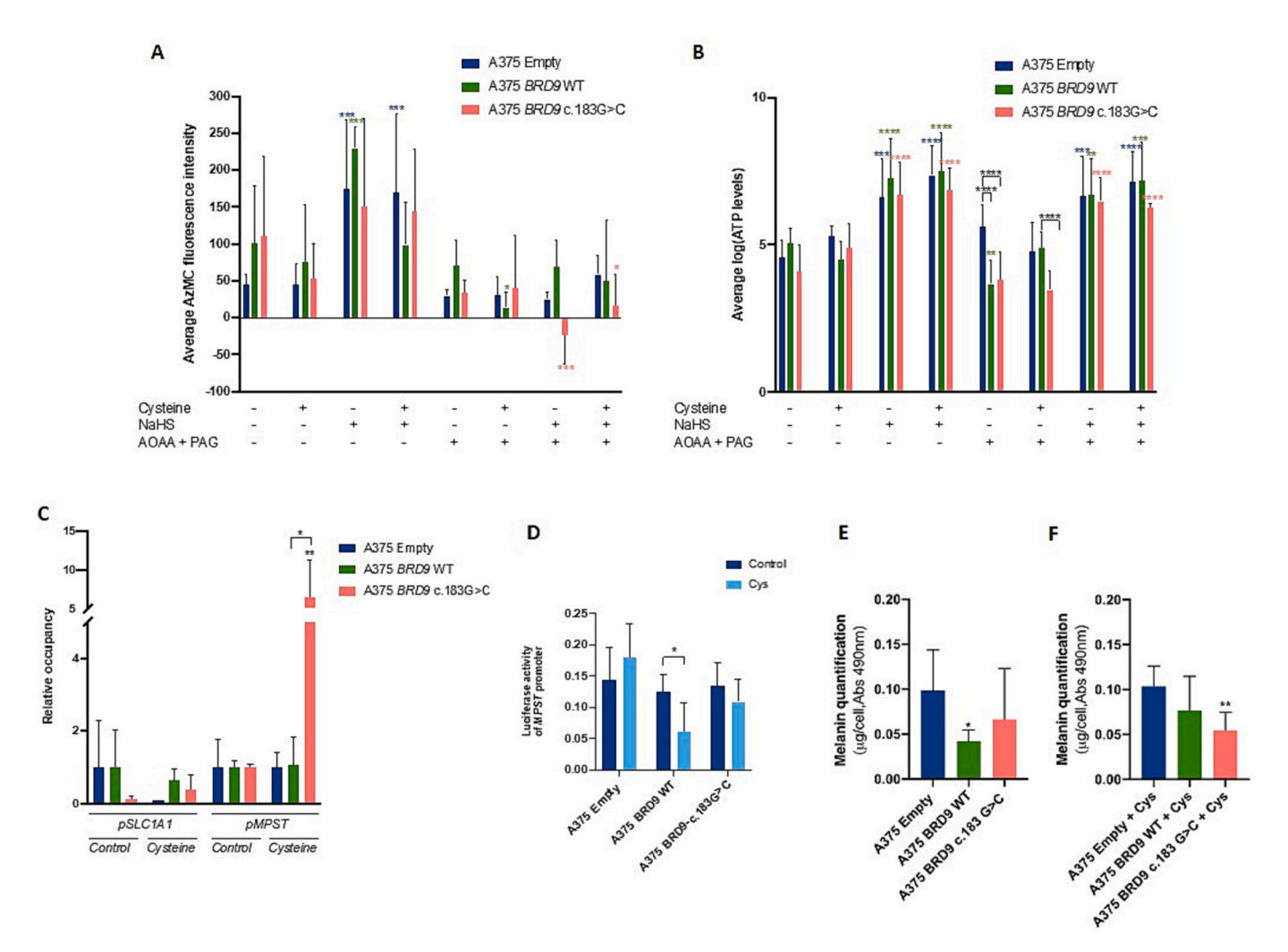
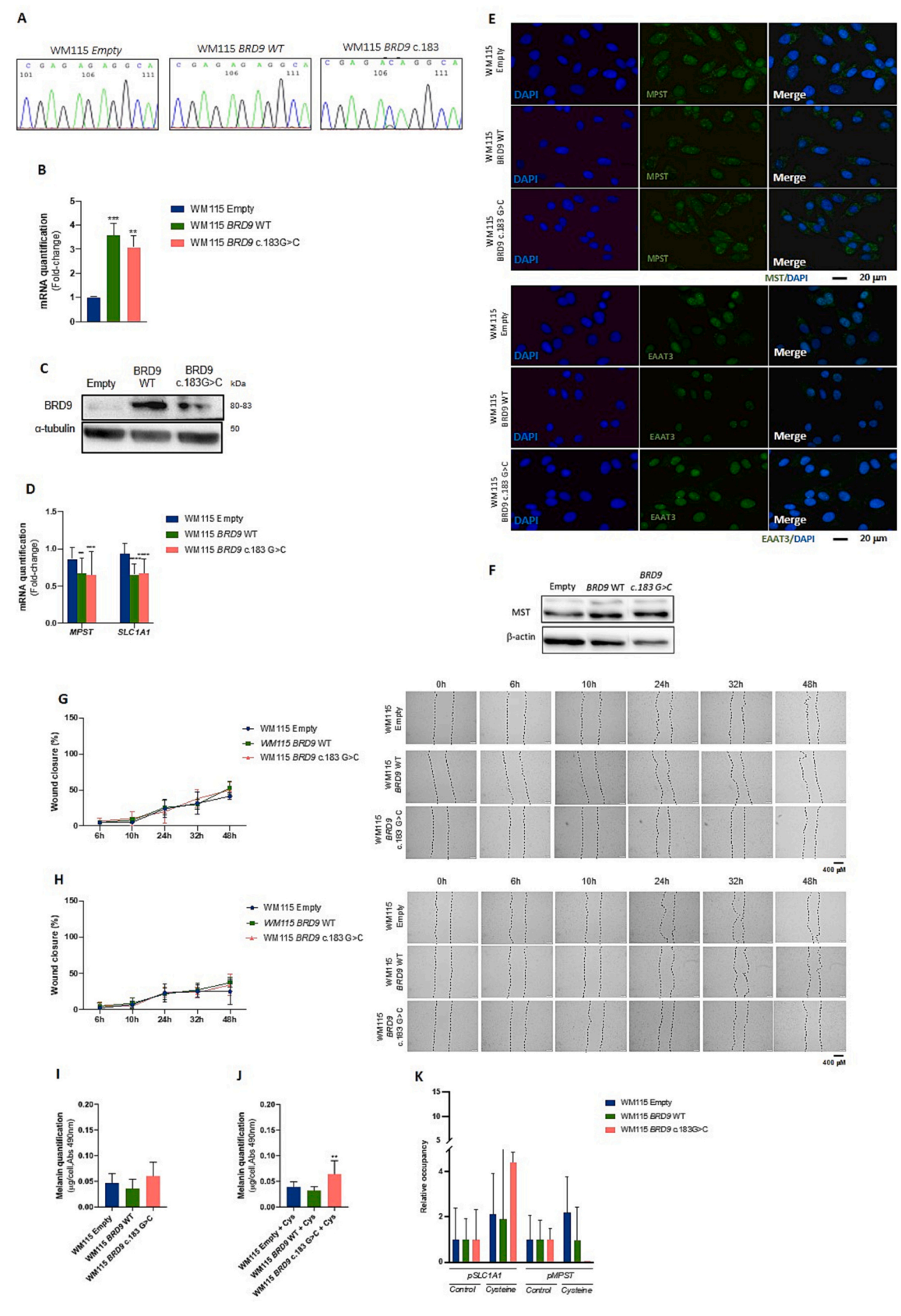


Fig. 4. BRD9 wild-type and BRD9 c.183G>C overexpression induces a more efficient H₂S-producing phenotype, which does not always correspond to accumulated ATP levels in A375 melanoma cells, and modulates MST and EAAT3 activity through NRF2, inducing a remodeling in the melanin production pathway. (A) H₂S quantification following 7-Azido-4-Methylcoumarin probe (AzMC) signal indicates that A375 cells overexpressing BRD9 WT and BRD9 c.183 G>C, despite cysteine availability, show higher H₂S production, comparing to A375 Empty, independently of o-(carboxymethyl)hydroxylamine hemihydrochloride (AOAA) and dl-propargylglycine (PAG) treatment. NaHS treatment further increased H₂S levels in every cell line tested, irrespectively of co-incubation with cysteine. (B) ATP measurement in transfected A375 cells did not show a modulation of energy production by neither BRD9 WT nor BRD9 c.183 G>C overexpression, despite increased H₂S levels. NaHS alone or in combination with cysteine but not cysteine alone led to increased ATP levels across the three cell lines. (C) ChIP analysis show a high binding of NRF2 to MPST promoter in the presence of cysteine. (D) Transfection of A375 melanoma cells with BRD9 WT induces decreased MPST promoter activity in the presence of cysteine. Melanin quantification in the absence (E) and presence (F) of cysteine was performed and cysteine exposure. Melanin quantification show decreased levels in A375 overexpressing-BRD9 WT in the absence of cysteine, but also decrease A375 BRD9 c.183 G>C melanin production in the presence of cysteine. Data is represented as mean \pm SD. *p < 0.5, **p < 0.01, ****p < 0.001, ****p < 0.0001. Experiments were performed with biological triplicates.

cysteine did not affect the development of tumors but the overexpression of BRD9 c.183 G>C induced tumors with statistically significant higher thickness and marked invasion edge comparing to A375 control and BRD9 WT.

3.8. Inhibition of MST induces a significant decrease in A375 and WM115 cell viability

Since our results pointed to MST as a crucial player in the rewiring of metabolic and cellular features of A375 overexpressing *BRD9* WT and



(caption on next page)

Fig. 5. Overexpression of BRD9 WT and BRD9 c.183G>C was successfully induced in WM115 cells and modulates the expression of MPST/MST and SLC1A1/EAAT3, leading to deregulated melanin production in the presence of cysteine. By Sanger sequencing the sequence mRNA was confirmed (A) and by qPCR (B) and western blotting (C) the transfection of WM115 melanoma cells and the expression of the BRD9 variants was confirmed WM115 cells transfection with wild-type over-expression and BRD9 c.183G>C (over)expression vectors induced increased mRNA and protein levels of BRD9, comparing to empty vector. (D-E) qPCR and immunofluorescence analysis indicate that BRD9 WT and c.183G>C overexpression induces decreased MPST/MST and SLC1A1/EAAT3 expression in WM115. (F) Western blotting for MST expression. (G) BRD9 WT/c.183G>C overexpression do not induce effects in WM115 migration, by wound healing, in the absence of cysteine. (H) BRD9 WT/c.183G>C overexpression does not induce effects in WM115 migration, by wound healing, in the presence of cysteine. Melanin quantification in the absence (I) and presence (J) of cysteine was performed and cysteine exposure increased melanin levels in BRD9 c.183G>C WM115 cells. (K) ChIP analysis show that NRF2 does not bind to MPST or SLC1A1 promoter in the absence nor presence of cysteine in WM115 cell variants. Data is represented as mean \pm SD. *p < 0.5, **p < 0.01, ****p < 0.001, ****p < 0.001. Experiments were performed with biological triplicates.

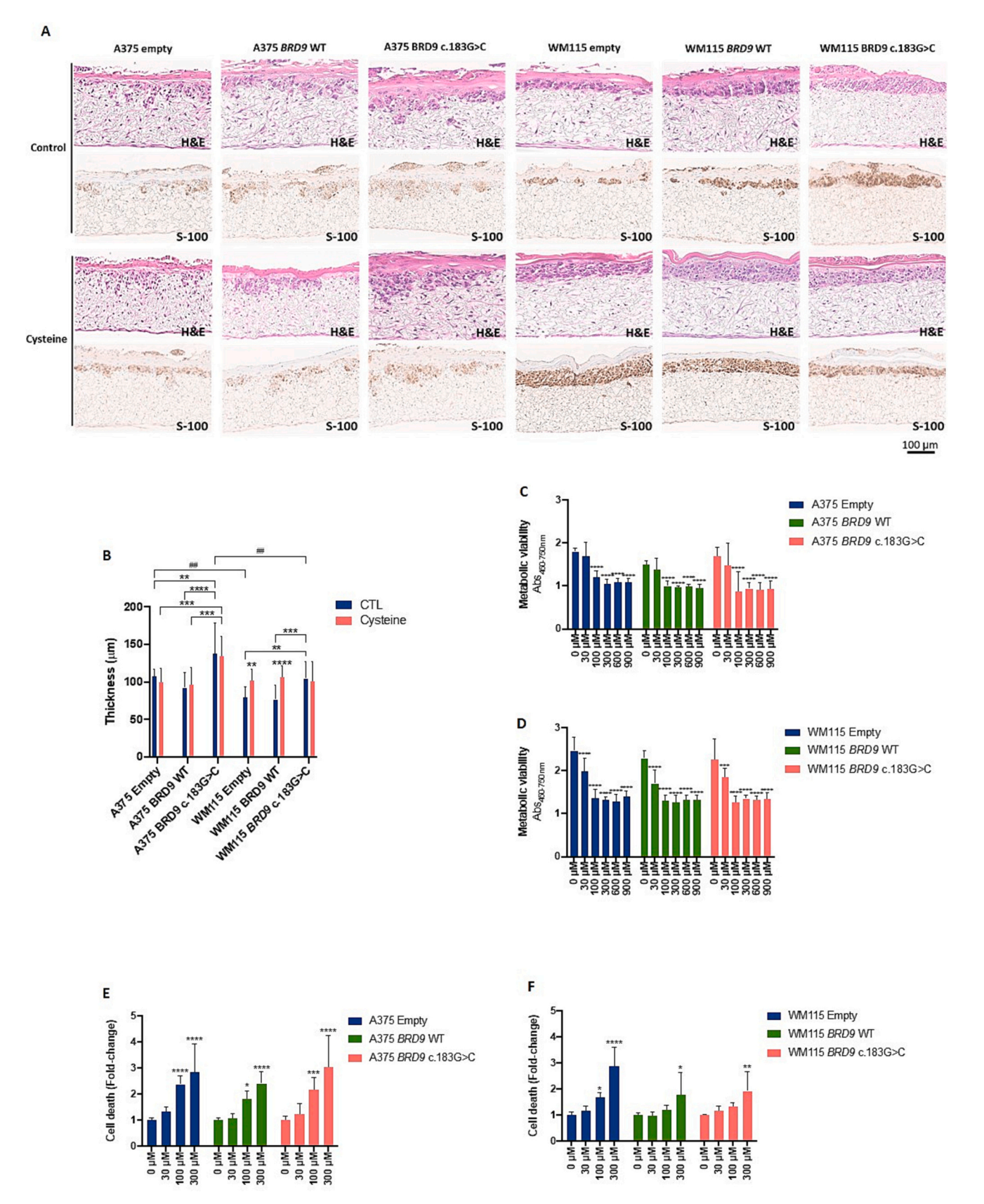
BRD9 c.183 G>C; and also WM115 express high basal levels of MST independently of *BRD9* status, we supposed that MST can be a target in these melanoma models. Therefore, Empty, *BRD9* WT and *BRD9* c.183 G>C variants of A375 and WM115 were exposed to increasing concentrations of an MST chemical inhibitor for 48 h. A375 *BRD9* WT/c.183 G>C and WM115 *BRD9* WT/c.183 G>C showed similar responses to the inhibitor, with a more significant viability decrease between the concentrations of 30 to 100 μM of the inhibitor (Fig. 6C, D, E and F). Furthermore, upon exposure to the MST inhibitor, A375 presents a higher EC_{50} comparing to WM115, corroborating a different reliance of both cell lines on MST (Supplementary Fig. S1). Both cell lines expressing BRD9 (WT and c.183 G>C) displayed lower EC_{50} with respect to the 'empty' parent lines, confirming the BRD9 modulation of MPST expression.

4. Discussion

Hereditary CM constitutes a significant part of all CM cases, in which most of the diagnoses remain without a known genetic familial cause. It is, thus, crucial to explore and acknowledge novel genetic targets that can be associated with CM familial history and that can explain increased susceptibility. To our knowledge, this is the first study exploring the molecular effects of the BRD9 c.183G>C variant in melanoma. Our study indicates that this variant, even though predicted to be benign rather than disease-causing (Fig. 1), induces different alterations in the CM cell lines tested, A375 and WM115. According to Sanger COSMIC database [97] A375 cells present a different genetic background from WM115, presenting mutated BRAF (c.1799T>A, p. V600E) and CDKN2A (c.181G>T, p.E61*; c.205G>T, p.E69*), while WM115 presents mutated BRAF (c.1799 1800TG>AT, p.V600D), CDKN2A (c.1 150del150, p.?) and PTEN (c.493 634del142, p.?), presenting deletions in both CDKN2A and PTEN. The significantly different genetic background of A375 and WM115 cells can explain the distinct effect of overexpressing BRD9 WT and mutated variants. In fact, it is already described that coexisting BRAF and PTEN mutations are directly linked to metastatic melanoma [98]. Importantly, in this study we disclosed BRD9 role as a regulator of cysteine metabolism. The involvement of NRF2 in the increased expression of MPST gene, as we verified that NRF2 binding to MPST promoter in A375 BRD9 c.183 G>C is increased and stimulated by cysteine (Fig. 4C), is in agreement with BRD9 and SWI/SNF loss of function, already described in NSCLC [70]. Importantly, new studies are needed to determine the impact of c.183 G>C in BRD9 structure and function, in order to understand the way this BRD9 mutaed variant can interfere with SWI/SNF complex function and somehow differentially modulate the expression of genes. Despite the structurally and chemically conservative substitution of glutamate by aspartate resulting from this mutation, the impact on its structure is reinforced by the inability of PROTAC BRD9 degrader-1 to deplete the mutated variant in A375 cells (Fig. 3H and J). Indeed, both BRD9 WT and c.183G>C induced distinct metabolic profiles, with emphasis on amino acid metabolism (Fig. 2H, I and J; Fig. 3A, B and C). Different genetic backgrounds induce cellular diversity, and our in vitro models can represent two distinct melanoma profiles: a cysteine remodeled metabolic profile by BRD9 with increased MST expression leading to a more invasive phenotype, and a molecular profile with decreased

expression of MST induced by BRD9 altered status, with no influence in cell migration. Therefore, the BRD9 c.183G>C variant associates to a significantly more migratory phenotype in A375 cells (Fig. 2G), but not in WM115 cells, which maintained their migratory capacity independently of the BRD9 status (Fig. 5G). The role of mutant in melanoma was confirmed in the increased invasive capacity exhibited by A375 BRD9 c.183G>C variant (Fig. 6A and B). This highlights the possibility that BRD9 may not be so relevant in terms of migration in WM115 cells comparing to A375 cells. A detail that likely accounts for this observation is the fact that WM115 cells have the deletion of the E-cadherin encoding gene. It was previously shown that E-cadherin re-expression in melanoma cells decreases the migratory and invasive capacity of cells and rescues the ability of cell-to-cell binding [99]. Despite the fact that A375 cells show higher migration rates in their basal state than WM115 cells (Figs. 2G, 5G), WM115 cells have loss of E-cadherin function, hampering finding differences between the migratory capacities of these cell line variants. Furthermore, and looking at the interference of cysteine metabolic adaptation in cell migration, all WM115 cell variants migrate at a lower rate in the presence of cysteine comparing to control conditions (Fig. 5G and H). The opposite was observed in A375 cell line, in which A375 BRD9 c.183G>C cell variant exposed to cysteine migrates at a higher rate than in control conditions (Fig. 2F and G). The 3D skin model revealed that A375 cell line is more invasive than WM115 cell line, which besides presenting tumors, cells do not invade (Fig. 6A and B). However, upon cysteine exposure, WM115 control and BRD9 WT formed statistically significant thicker tumors than in the absence of cysteine. By comparing the metabolic viability of all cell variants, it was verified that WM115 cells present higher values than A375 variants, in control conditions. This possibly indicates that WM115 cells proliferate at a higher rate than A375 cells (Fig. 6D and E), and this will contribute for the increased thickness of WM115 melanomas in 3D skin model, suggesting that cysteine exposure may stimulate WM115 proliferation. Considering the A375 variants, the exposure to cysteine did not affect the development of tumors but the overexpression of BRD9 c.183 G>C induced tumors with statistically significant higher thickness and marked invasion edge comparing to A375 control and BRD9 WT (Fig. 6A

Cysteine exposure induced decreased levels of glutamate in both A375 Empty and BRD9 c.183G>C, which was accompanied by undetectable glutamine levels. However, in A375 BRD9 WT, cysteine led to an increasing tendency of glutamate and glutamine levels (Fig. 3A). Decreased levels of glutamate and glutamine can be explained by increased synthesis of glutathione, as described in ovarian cancer [53]. Glutathione's antioxidant role depends on cysteine's reactive thiol group [100]. Indeed, we found increased GSH levels in A375 Empty but not in A375 BRD9 c.183G>C. Instead, this variant showed a tendency towards decreased GSH levels in the presence of cysteine, as observed in cells expressing the A375 BRD9 WT variant (Fig. 3A). Decreased glutathione levels can derive from a slow glutathione synthesis and/or fast GSH consumption. However, the results point towards increased metabolic demands of BRD9 expressing cell variants, presenting a more demanding redox turnover, prompting the consumption of reduced glutathione, in contrast to a lower metabolic flow of A375 Empty cells. This is also supported by the evident signs of oxidative stress presented by A375 BRD9 c.183G>C cells, such as increased expression of the antioxidant



(caption on next page)

Fig. 6. BRD9 c.183G>C increased the invasiveness of A375 in a 3D *in vitro* skin model, and MST inhibition impacts on metabolic viability in all variants of A375 and WM115 cells. The effect of BRD9 WT and BRD9 c.183G>C overexpression in melanoma cell lines was evaluated in a 3D *in vitro* skin model. (A) Representative images of *in vitro* tumors in hematoxylin and eosin (H&E) staining and S-100 protein immunohistochemistry to specifically detect melanoma cells, and (B) the quantification of tumor thickness are presented, considering 20 imaging spots per slide of the 2 biological replicates. The impact of MST inhibition was assessed in A375 and WM115 BRD9 WT and BRD9 c.183G>C variants. Statistical significance between different conditions within each cell line (*) and between cell lines (#) were considered. By WST-1 assay (subtracting the absorbance measured at 480 nm and 760 nm), it was verified that MST inhibitor (I3MT-3) induces a significant decrease in metabolic viability of A375 (C) and WM115 (D) BRD9 WT and BRD9 c.183G>C variants, upon 48 h of exposure, with more significant viability decrease between the concentrations of 30 to 100 μ M of the inhibitor. The cell death, measured by flow cytometry (Annexin V-FITC and PT labeling), induced by I3MT-3 in all A375 (E) and WM115 (F) variants upon 48 h of exposure show differences in resistance to this treatment between A375 and WM115 empty variants versus variants overexpressing BRD9 WT and BRD9 c.183G>C: empty variants of both A375 and WM115 showed more resistance to the inhibitor and presented higher EC₅₀ values comparing to BRD9 WT and BRD9 c.183G>C: variants. Data is represented as mean \pm SD. *p < 0.5, ***/** p < 0.001, ****p < 0.0001. Experiments were performed with biological triplicates.

enzyme MST [101] and EAAT3 transporter (Fig. 3D, E and F). This is in line with our results regarding the enzymatic activity study in all three variants of A375. In fact, we found that A375 BRD9 c.183G>C cells exhibit increased steady-state levels of H₂S comparing to A375 Empty, in control conditions. Interestingly, A375 BRD9 WT, even though showing significant decreased expression of antioxidant enzymes and transporters, show similarly increased H₂S levels, comparing to A375 BRD9 c.183G>C (Fig. 4A), which can either indicate an increased H₂S production or a lower detoxifying ability. H₂S is described to act in two equally important ways: either as a potent antioxidant or as source of electron equivalents to the mETC, leading to ATP production [57,102]. In our results, increased H₂S levels do not translate in increased ATP levels (Fig. 4B). This may mean that BRD9 overexpression whether in its WT or mutated form can further induce imbalances in H₂S production as a distinct way to overcome oxidative stress.

Since complete culture medium contains glutamine, we expected to detect this amino acid in our metabolomics study. Low (A375 BRD9 WT) or inexistent (A375 Empty and A375 BRD9 c.183 G>C) levels of glutamine, independently of cysteine availability, further indicate high uptake and consumption of this amino acid (Fig. 3A). Decreased glutamine is associated with a necessity for redox control within the cell, and is usually found during catabolic stress and antioxidant imbalance [103]. Glutamine can act either as a positive or negative redox status modulator, depending on the activation of specific transcription factors triggered by stressful microenvironments [103]. In this case, high consumption of glutamine may act as an attempt by the cell to compensate the decreased GSH production due to cysteine diversion to other pathways, since these cells probably show increased ROS levels. Decreased glutathione levels are also described to be associated with decreased proliferation rates [103], which is in accordance with our results (Fig. 2D and E). Glycine levels drastically decrease in the presence of cysteine (Fig. 3A). Again, decreased availability of glycine may indicate a cellular response to oxidative stress, since glycine is also a component of glutathione. Moreover, the decreased levels of serine may indicate increased glycine synthesis and altogether highlight that glycine turnover is in operation in A375 BRD9 c.183 G>C cell variant.

We further observed a decrease in methionine levels in A375 Empty and BRD9 c.183 G>C when exposed to cysteine and in A375 BRD9 WT, independently of cysteine presence (Fig. 3A). Decreased methionine levels in the presence of cysteine suggest that exogenous cysteine stimulates methionine demethylation, with the resulting homocysteine either being remethylated back to methionine or entering the reverse transsulfuration pathway (RTP, comprising CBS and CSE). The observation that both A375 Empty and BRD9 c.183 G> variants express high levels of EAAT3, CBS and CSE-encoding genes favors the latter fate involving the RTP and leading to cysteine production (Fig. 3D, E and F). A375 BRD9 WT show low levels of methionine, unaffected by cysteine availability (Fig. 3A), probably related to low CBS expression by this variant. This A375 variant likely relies on a different source of cysteine, since H_2S steady-state levels are comparable to A375 BRD9 c.183 G>C in control conditions (Fig. 4A). Decreased levels of acetate (Fig. 3B) are in agreement with decreased proliferation rate [104,105] in cells overexpressing BRD9 (Fig. 2D and E), independently of the mutational status. Indeed, the average number of cells between time point 10 h and 16 h is significantly lower in A375 *BRD9* c.183 G>C comparing to A375 *BRD9* WT. Decreased levels of choline and phosphocholine can also be indicative of a decreased proliferation rate [106,107] (Fig. 3 C; Fig. 2D and E). Additionally, high levels of formate and lactate may be related to increased invasion, independently of cysteine presence [108,109] (Figs. 3B; 2F and G).

Cysteine metabolism is deeply associated with increased tumor aggressiveness as described before, and so, we hypothesize that BRD9induced cysteine metabolic remodeling may be an extremely relevant feature to further disclose in malignant CM. In fact, our results suggest that BRD9 WT has an inhibitory effect on MPST expression and the mutated BRD9 variant exhibits the opposite effect by upregulating MPST, as verified at the RNA as protein level (Fig. 3). Cysteine, besides being able to supply energy to cancer cells, can also provide them with the resistance mechanisms to overlap standard therapy regimens applied to cancer patients. Moreover, it is a pivotal intervenient in pheomelanin production. Thus, increased cysteine metabolism and uptake can intervene in different ways, all of them contributing to tumorigenesis and/or tumor progression. We postulate that overexpression of WT or c.183G>C BRD9 can contribute to imbalances in melanin production, deregulating the eumelanin/pheomelanin ratio, thus leading to a higher susceptibility to CM development. In fact, while eumelanin exerts a photo/radioprotection role, pheomelanin can be a source of mutagenic events upon radiation exposure [34,110]. Several studies have uncovered that, indeed, pheomelanin can be associated with increased production of ROS upon UVR exposure [110-113]. Moreover, imbalances in this ratio are already described in uveal melanoma cells, which show much higher levels of pheomelanin than eumelanin [114].

Metabolic rewiring has become clear to have a central role in tumor development, progression and resistance and has, in fact, been considered a core hallmark of cancer [115]. Thus, it is essential to further explore the role of BRD9 as a CM susceptibility gene but also as a metabolic regulator. The present work opens a new door towards understanding hereditary melanoma as a complex entity, in which tumor, not only genetic but also metabolic profiling may be a central piece to disentangle familial history and cancer susceptibility, as well as an important therapy response predictor. Additionally, this study supports a broad role of MST enzyme as a crucial player in CM, not only in tumors presenting alterations in BRD9. In fact, our results show that inhibition of MST leads to a decrease in cell viability in both A375 and WM115 cell lines, with a significantly more pronounced effect in A375 and WM115 variants overexpressing BRD9 WT or c.183 G>C, presenting lower EC₅₀ values for the latter (Fig. 6C, D, E and F). Indeed, increasing evidence points towards MST as a player in cancer metabolic remodeling and its encoding gene, MPST, though constitutively expressed in normal differentiated cells, is also often found overexpressed in several different cancer cell lines as well as across a wide range of tumors [55,116]. Moreover, studies have correlated increased expression of MST with chemoresistance in different cancer types [117,118] and have revealed the crucial role of MST in cancer cell proliferation [119–121]. We have previously suggested a critical role for MST expression and activity in cancer according to cancer type and metabolic context, with emphasis

on its role in carcinogenesis and/or cancer progression [55]. In this study, we disclosed a putative role of MST in the metabolic reliance of BRD9-mutated CM. MST elevated expression can define a parameter regarding CM aggressiveness, being associated with more migratory and invasive but less proliferative phenotypes, with low melanin production, thus characterizing a specific subset of CM. More experiments to characterize the mechanism underlying the effect of mutated BRD9 should be performed, to better understand the function of the mutated protein.

5. Conclusion

BRD9 is a CM-associated gene with yet much potential to be further explored, namely in larger cohorts of CM patients in familial and sporadic contexts. This study highlights that not only the mutational status of BRD9 but also its expression level can be used as a marker for CM aggressiveness. Here, BRD9 was disclosed as a regulator of cysteine metabolism in a CM in vitro model. Overexpression of BRD9 in its WT or c.183G>C variants can induce metabolic remodeling, leading to altered cellular features. BRD9 c.183G>C, thus, introduces cysteine metabolism as a putative central player in CM susceptibility, as well as in CM progression. Overall, we demonstrated that A375 cell line aggressiveness correlates with the overexpression of MST and EAAT3, in a mutated BRD9-dependent way. Because cysteine also conditions the production of melanin forms, the increased expression of EAAT3 may contribute for more pheomelanin production, which has a lower protective effect against the mutagenic effect of UV radiation. On the one hand, cysteine catabolism through MST allows the use of cysteine as an energetic and synthetic source; on the other hand, the increased intracellular bioavailability favors the production of pheomelanin, resulting in lower protection against UV damage. Moreover, we disclosed a putative mechanism linking mutated forms of BRD9 to susceptibility to melanomagenesis. This study opens new perspectives to reinforce the need to explore the impact of c.183 G>C mutation in the conformation and function of BRD9 protein, and ultimately in the transcriptional complexes to which BRD9 belong that will greatly influence gene modulation and control cancer behavior. Disclosing these alterations will help defining the role of BRD9 in cutaneous melanoma. Furthermore, cysteine metabolism is a hub for innovative strategies to fight cancer, as it is a core net of metabolic pathways essential to sustain cancer cells survival and the mechanisms supporting aggressiveness and disease progression. Therefore, MST can be a suitable marker for CM aggressiveness and a potential target, since it correlates with increased migratory and invasive potential and decreased production of melanin, accounting for an increased risk of accumulating mutations due to decreased DNA protection against radiation.

Supplementary data to this article can be found online at https://doi. org/10.1016/j.bbadis.2023.166983.

Funding

The institutions are funded by Fundação para a Ciência e a Tecnologia/Ministério da Ciência, Tecnologia e Ensino Superior (FCT/MCTES, Portugal) through national funds to iNOVA4Health (UIDB/04462/2020 and UIDP/04462/2020), to MOSTMICRO-ITQB (UIDB/04612/2020 and UIDP/04612/2020) and the Associated Laboratory LS4FUTURE (LA/P/0087/2020). Ana Hipólito PhD fellowship was funded by FCT (SFRH/BD/148441/2019). Ana Tomás PhD fellowship was funded by FCT (2021.06204.BD). Luís C. Cabaço PhD fellowship was funded by FCT (2020.08812.BD). Luís G. Gonçalves was financed by an FCT contract according to DL57/2016, [SFRH/BPD/111100/2015]. Marta Pojo was supported by Liga Portuguesa Contra o Cancro – Núcleo Regional do Sul (LPCC-NRS). This work benefited from access to CERMAX, ITQB-NOVA, Oeiras, Portugal with equipment funded by FCT, project AAC 01/SAICT/2016.

CRediT authorship contribution statement

AH- wrote the 1st draft of the paper, planned and performed the most experiments, revised and discussed the paper; RX- performed NGS analysis of melanoma samples and analysis of mutated variants, revised and discussed the paper; CB and AT- established stable transduced cell lines, revised and discussed the paper; IL- performed NMR and immunofluorescence analysis, revised and discussed the paper; LCC- performed 3D skin model experiments, revised and discussed the paper; FSresponsible for the 3D skin models processing and IHC analysis, revised and discussed the paper; AO- guide the optimization procedures of the 3D skin models, revised and discussed the paper; DCB- coordinated and supervised the 3D skin models, revised and discussed the paper; JBVsupervised hydrogen sulfide measurement and enzymatic experiments, revised and discussed the paper; LGG- coordinated NMR spectroscopy analysis, revised and discussed the paper; MP- coordinated and supervised the patients samples analysis and cell line variants establishment, responsible for funding, revised and discussed the paper; JS- coordinated and supervised the cancer biology and metabolism project components, responsible for funding, revised and discussed the paper.

Declaration of competing interest

The authors declare the following financial interests/personal relationships which may be considered as potential competing interests: Ana Hipólito reports financial support was provided by Foundation for Science and Technology. Isabel Lemos reports financial support was provided by Foundation for Science and Technology.

Data availability

https://www.ncbi.nlm.nih.gov/pmc/articles/PMC7230562/

References

- A. Sandru, S. Voinea, E. Panaitescu, A. Blidaru, Survival rates of patients with metastatic malignant melanoma, J. Med. Life 7 (2014) 572.
- [2] Y. Sang, Y. Deng, Current insights into the epigenetic mechanisms of skin cancer, Dermatol. Ther. (2019), https://doi.org/10.1111/DTH.12964.
- [3] L.M. Parra, R.M. Webster, The malignant melanoma market, Nat. Rev. Drug Discov. (2022), https://doi.org/10.1038/D41573-022-00075-5.
- [4] S. Santourlidis, W.A. Schulz, M.J. Araúzo-Bravo, D. Gerovska, P. Ott, M. L. Bendhack, et al., Epigenetics in the diagnosis and therapy of malignant melanoma, Int. J. Mol. Sci. 23 (2022) 23.
- [5] N. Wasif, S.P. Bagaria, P. Ray, D.L. Morton, Does metastasectomy improve survival in patients with stage IV melanoma? A cancer registry analysis of outcomes, J. Surg. Oncol. 104 (2011) 111.
- [6] S.R. Palmer, L.A. Erickson, I. Ichetovkin, D.J. Knauer, S.N. Markovic, Circulating serologic and molecular biomarkers in malignant melanoma, Mayo Clin. Proc. 86 (2011) 981–990.
- [7] A.M.M. Eggermont, C.U. Blank, M. Mandalà, G.V. Long, V.G. Atkinson, S. Dalle, et al., Adjuvant pembrolizumab versus placebo in resected stage III melanoma (EORTC 1325-MG/KEYNOTE-054): distant metastasis-free survival results from a double-blind, randomised, controlled, phase 3 trial, Lancet Oncol. 22 (2021) 643-654
- [8] M.G. Franken, B. Leeneman, M.J.B. Aarts, A.C.J. van Akkooi, F.W.P.J. van den Berkmortel, M.J. Boers-Sonderen, et al., Trends in survival and costs in metastatic melanoma in the era of novel targeted and immunotherapeutic drugs, ESMO Open. 6 (2021), 100320.
- [9] L.B. Alexandrov, S. Nik-Zainal, D.C. Wedge, S.A.J.R. Aparicio, S. Behjati, A. V. Biankin, et al., Signatures of mutational processes in human cancer, Nature 500 (2013) 415–421.
- [10] X. Sun, N. Zhang, C. Yin, B. Zhu, X. Li, Ultraviolet radiation and melanomagenesis: from mechanism to immunotherapy, Front. Oncol. 10 (2020) 951.
- [11] F. Dimitriou, R. Krattinger, E. Ramelyte, M.J. Barysch, S. Micaletto, R. Dummer, et al., The world of melanoma: epidemiologic, genetic, and anatomic differences of melanoma across the globe, Curr. Oncol. Rep. (2018), https://doi.org/10.1007/S11912-018-0732-8.
- [12] B.K. Armstrong, A.E. Cust, Sun exposure and skin cancer, and the puzzle of cutaneous melanoma: a perspective on Fears et al. Mathematical models of age and ultraviolet effects on the incidence of skin cancer among whites in the United States. American Journal of Epidemiology 1977; 105: 420–427, Cancer Epidemiol. 48 (2017) 147–156.

- [13] C.J. Hussussian, J.P. Struewing, A.M. Goldstein, P.A.T. Higgins, D.S. Ally, M. D. Sheahan, et al., Germline p16 mutations in familial melanoma, Nat. Genet. 8 (1994) 15–21.
- [14] A. Kamb, D. Shattuck-Eidens, R. Eeles, Q. Liu, N.A. Gruis, W. Ding, et al., Analysis of the p16 gene (CDKN2) as a candidate for the chromosome 9p melanoma susceptibility locus, Nat. Genet. 8 (1994) 22–26.
- [15] F.W. Huang, E. Hodis, M.J. Xu, G.V. Kryukov, L. Chin, L.A. Garraway, Highly recurrent TERT promoter mutations in human melanoma, Science 339 (2013) 957-959
- [16] S. Horn, A. Figl, P.S. Rachakonda, C. Fischer, A. Sucker, A. Gast, et al., TERT promoter mutations in familial and sporadic melanoma, Science 339 (2013) 050, 061
- [17] C.D. Robles-Espinoza, M. Harland, A.J. Ramsay, L.G. Aoude, V. Quesada, Z. Ding, et al., POT1 loss-of-function variants predispose to familial melanoma, Nat. Genet. 46 (2014) 478–481.
- [18] J. Shi, X.R. Yang, B. Ballew, M. Rotunno, D. Calista, M.C. Fargnoli, et al., Rare missense variants in POT1 predispose to familial cutaneous malignant melanoma, Nat. Genet. 46 (2014) 482–486.
- [19] S. Bassoli, C. Pellegrini, C. Longo, L. Di Nardo, F. Farnetani, A.M. Cesinaro, et al., Clinical, dermoscopic, and confocal features of nevi and melanomas in a multiple primary melanoma patient with the MITF p.E318K homozygous mutation, Melanoma Res. 28 (2018) 166–169.
- [20] N.R. Adler, J.W. Kelly, A. Haydon, C.A. McLean, V.J. Mar, Clinicopathological characteristics and prognosis of patients with multiple primary melanomas, Br. J. Dermatol. 178 (2018) e44–e45.
- [21] C. Campos, S. Fragoso, R. Luís, F. Pinto, C. Brito, S. Esteves, et al., High-throughput sequencing identifies 3 novel susceptibility genes for hereditary melanoma, Genes (Basel) 11 (2020) 403.
- [22] X. Wang, S. Wang, E.C. Troisi, T.P. Howard, J.R. Haswell, B.K. Wolf, et al., BRD9 Defines a SWI/SNF Sub-complex and Constitutes a Specific Vulnerability in Malignant Rhabdoid Tumors 10, 2019, pp. 1–11.
- [23] Tran, K. D., Chakravarty, T., Garzon, J. L., Saraf, A., Florens, L., Washburn, M. P., et al. Hypoxic Response is Driven by the BAF Form of SWI/SNF. https://doi.org/10.1101/2022.02.16.480689.
- [24] X. Wang, J.R. Haswell, C.W.M. Roberts, Molecular pathways: SWI/SNF (BAF) complexes are frequently mutated in cancer—mechanisms and potential therapeutic insights, Clin. Cancer Res. 20 (2014) 21–27.
- [25] A. Van Vaart, Vaart Der, A. Van Der, M. Godfrey, V. Portegijs, S. Van Den Heuvel, Dose-dependent functions of SWI/SNF BAF in permitting and inhibiting cell proliferation in vivo, Sci. Adv. (2020), https://doi.org/10.1126/SCIADV. AAV2022
- [26] J.J. Smith, Y. Xiao, N. Parsan, T.N. Medwig-Kinney, M.A.Q. Martinez, F.E. Q. Moore, et al., The SWI/SNF chromatin remodeling assemblies BAF and PBAF differentially regulate cell cycle exit and cellular invasion in vivo, PLoS Genet. (2022), https://doi.org/10.1371/JOURNAL.PGEN.1009981.
 [27] X. Wang, S. Wang, E.C. Troisi, T.P. Howard, J.R. Haswell, B.K. Wolf, et al., BRD9
- [27] X. Wang, S. Wang, E.C. Troisi, T.P. Howard, J.R. Haswell, B.K. Wolf, et al., BRD9 Defines a SWI/SNF Sub-complex and Constitutes a Specific Vulnerability in Malignant Rhabdoid Tumors 10, 2019, pp. 1–11.
- [28] J. Gatchalian, S. Malik, J. Ho, D.S. Lee, T.W.R. Kelso, M.N. Shokhirev, et al., A non-canonical BRD9-containing BAF chromatin remodeling complex regulates naive pluripotency in mouse embryonic stem cells, Nat. Commun. 91 (9) (2018) 1–16.
- [29] H. Huang, Y. Wang, Q. Li, X. Fei, H. Ma, R. Hu, miR-140-3p functions as a tumor suppressor in squamous cell lung cancer by regulating BRD9, Cancer Lett. 446 (2019) 81–89
- [30] W. Lou, K. Gao, C. Xu, Q. Li, Bromodomain-containing protein 9 is a prognostic biomarker associated with immune infiltrates and promotes tumor malignancy through activating notch signaling pathway in negative HIF-2α clear cell renal cell carcinoma, IUBMB Life 73 (2021) 1334–1347.
- [31] C. Dou, L. Sun, L. Wang, J. Cheng, W. Wu, C. Zhang, et al., Bromodomain-containing protein 9 promotes the growth and metastasis of human hepatocellular carcinoma by activating the TUFT1/AKT pathway, Cell Death Dis. (2020), https://doi.org/10.1038/S41419-020-02943-7.
- [32] D. Fang, M.R. Wang, J.L. Guan, Y.Y. Han, J.Q. Sheng, D.A. Tian, et al., Bromodomain-containing protein 9 promotes hepatocellular carcinoma progression via activating the Wnt/β-catenin signaling pathway, Exp. Cell Res. (2021), https://doi.org/10.1016/J.YEXCR.2021.112727.
- [33] N. Barma, T.C. Stone, L.M.C. Echeverria, S. Heavey, Exploring the value of BRD9 as a biomarker, therapeutic target and co-target in prostate cancer, Biomolecules (2021), https://doi.org/10.3390/BIOM11121794/S1.
- [34] R.M. Slominski, T. Sarna, P.M. Płonka, C. Raman, A.A. Brożyna, A.T. Slominski, Melanoma, melanin, and melanogenesis: the yin and yang relationship, Front. Oncol. 12 (2022) 1.
- [35] N. Kobayashi, A. Nakagawa, T. Muramatsu, Y. Yamashina, T. Shirai, M. W. Hashimoto, et al., Supranuclear melanin caps reduce ultraviolet induced DNA photoproducts in human epidermis, J. Invest. Dermatol. 110 (1998) 806–810.
- [36] T.H. Nasti, L. Timares, MC1R, eumelanin and pheomelanin: their role in determining the susceptibility to skin cancer, Photochem. Photobiol. 91 (2015) 188–200.
- [37] J.Y. Lin, D.E. Fisher, Melanocyte biology and skin pigmentation, Nature 445 (2007) 843–850.
- [38] D. Schadendorf, D.E. Fisher, C. Garbe, J.E. Gershenwald, J.J. Grob, A. Halpern, et al., Melanoma, Nat. Rev. Dis. Prim. (2015), https://doi.org/10.1038/ NRDP.2015.3.

- [39] X. Sun, N. Zhang, C. Yin, B. Zhu, X. Li, S. Chen, et al., Ultraviolet radiation and melanomagenesis: from mechanism to immunotherapy, Front. Oncol. 10 (2020) 951.
- [40] D.T. Bishop, F. Demenais, M.M. Iles, M. Harland, J.C. Taylor, E. Corda, et al., Genome-wide association study identifies three loci associated with melanoma risk, Nat. Genet. 41 (2009) 920–925.
- [41] A. Körner, J. Pawelek, Mammalian tyrosinase catalyzes three reactions in the biosynthesis of melanin, Science 217 (1982) 1163–1165.
- [42] A.B. Lerner, T.B. Fitzpatrick, Biochemistry of melanin formation, Physiol. Rev. 30 (1950) 91–126.
- [43] S. Ito, K. Wakamatsu, Melanin chemistry and melanin precursors in melanoma, J. Invest. Dermatol. 92 (1989) 261S–265S.
- [44] Nguyen, N. T., and David, F. MITF and UV Responses in Skin: From Pigmentation to Addiction. https://doi.org/10.1111/pcmr.12726.
- [45] E.J. Land, C.A. Ramsden, P.A. Riley, Pulse radiolysis studies of ortho-quinone chemistry relevant to melanogenesis, J. Photochem. Photobiol. B Biol. 64 (2001) 123–135.
- [46] E.J. Land, P.A. Riley, Spontaneous redox reactions of dopaquinone and the balance between the eumelanic and phaeomelanic pathways, Pigment Cell Res. 13 (2000) 273–277.
- [47] J.R. Jara, P. Aroca, F. Solano, J.H. Martinez, J.A. Lozano, The role of sulfhydryl compounds in mammalian melanogenesis: the effect of cysteine and glutathione upon tyrosinase and the intermediates of the pathway, Biochim. Biophys. Acta, Gen. Subj. 967 (1988) 296–303.
- [48] H. Rorsman, E. Albertsson, L.E. Edholm, C. Hansson, L. Ógren, E. Rosengren, Thiols in the melanocyte, Pigment Cell Res. 1 (1988) 54-60.
- [49] R. Luís, C. Brito, M. Pojo, Melanoma metabolism: cell survival and resistance to therapy, Adv. Exp. Med. Biol. 1219 (2020) 203–223.
- [50] J. Serpa, Metabolic remodeling as a way of adapting to tumor microenvironment (TME), a job of several holders, Adv. Exp. Med. Biol. 1219 (2020) 1–34.
- [51] N. Traverso, R. Ricciarelli, M. Nitti, B. Marengo, A.L. Furfaro, M.A. Pronzato, et al., Role of glutathione in cancer progression and chemoresistance, Oxidative Med. Cell. Longev. (2013), https://doi.org/10.1155/2013/972913.
- [52] R. Colla, A. Izzotti, C. De Ciucis, D. Fenoglio, S. Ravera, A. Speciale, et al., Glutathione-mediated antioxidant response and aerobic metabolism: two crucial factors involved in determining the multi-drug resistance of high-risk neuroblastoma, Oncotarget 7 (2016) 70715.
- [53] F. Lopes-Coelho, S. Gouveia-Fernandes, L.G. Gonçalves, C. Nunes, I. Faustino, F. Silva, et al., HNF1β drives glutathione (GSH) synthesis underlying intrinsic carboplatin resistance of ovarian clear cell carcinoma (OCCC), Tumour Biol. 37 (2016) 4813–4829.
- [54] E.V. Kalinina, N.N. Chernov, M.D. Novichkova, Role of glutathione, glutathione transferase, and glutaredoxin in regulation of redox-dependent processes, Biochem 79 (2014) 1562–1583.
- [55] A. Hipólito, S.C. Nunes, J.B. Vicente, J. Serpa, Cysteine Aminotransferase (CAT): A Pivotal Sponsor in Metabolic Remodeling and an Ally of 3-Mercaptopyruvate Sulfurtransferase (MST) in Cancer, 2020, https://doi.org/10.3390/ MOLECHIES25173984
- [56] K. Zuhra, C.S. Tomé, E. Forte, J.B. Vicente, A. Giuffrè, The multifaceted roles of sulfane sulfur species in cancer-associated processes, Biochim. Biophys. Acta Bioenerg. (2021), https://doi.org/10.1016/J.BBABIO.2020.148338.
- [57] A. Giuffrè, C.S. Tomé, D.G.F. Fernandes, K. Zuhra, J.B. Vicente, Hydrogen sulfide metabolism and signaling in the tumor microenvironment, Adv. Exp. Med. Biol. 1219 (2020) 335–353.
- [58] C. Szabo, C. Coletta, C. Chao, K. Módis, B. Szczesny, A. Papapetropoulos, et al., Tumor-derived hydrogen sulfide, produced by cystathionine-β-synthase, stimulates bioenergetics, cell proliferation, and angiogenesis in colon cancer, Proc. Natl. Acad. Sci. U. S. A. 110 (2013) 12474–12479.
- [59] J. Xiong, N. Wang, H.J. Zhong, B.W. Cui, S. Cheng, R. Sun, et al., SLC1A1 mediated glutamine addiction and contributed to natural killer T-cell lymphoma progression with immunotherapeutic potential, EBioMedicine (2021), https://doi.org/10.1016/J.EBIOM.2021.103614.
- [60] A. Cano-Galiano, A. Oudin, F. Fack, M.F. Allega, D. Sumpton, E. Martinez-Garcia, et al., Cystathionine-γ-lyase drives antioxidant defense in cysteine-restricted IDH1-mutant astrocytomas, Neuro-oncol. Adv. (2021), https://doi.org/10.1093/NOAJNL/VDAB057.
- [61] Y. Liu, L. Wang, X. Zhang, Y. Deng, L. Pan, H. Li, et al., A novel cystathionine γ-lyase inhibitor, 1194496, inhibits the growth and metastasis of human TNBC via downregulating multiple signaling pathways, Sci. Rep. (2021), https://doi.org/ 10.1038/\$41598-021-88355-9.
- [62] Y. Wang, J. Huang, W. Chen, R. Wang, M. Kao, Y. Pan, et al., Dysregulation of cystathionine γ-lyase promotes prostate cancer progression and metastasis, EMBO Rep. (2019), https://doi.org/10.15252/EMBR.201845986.
- [63] K. Zuhra, F. Augsburger, T. Majtan, C. Szabo, Cystathionine-β-synthase: molecular regulation and pharmacological inhibition, Biomolecules (2020), https://doi.org/10.3390/BIOM10050697.
- [64] E.A. Turbat-Herrera, M.J. Kilpatrick, J. Chen, A.T. Meram, J. Cotelingam, G. Ghali, et al., Cystathione β-synthase is increased in thyroid malignancies, Anticancer Res. 38 (2018) 6085–6090.
- [65] M. Feist, P. Schwarzfischer, P. Heinrich, X. Sun, J. Kemper, F. Von Bonin, et al., Cooperative STAT/NF-kB signaling regulates lymphoma metabolic reprogramming and aberrant GOT2 expression, Nat. Commun. (2018), https://doi.org/10.1038/S41467-018-03803-X.
- [66] R. Hong, W. Zhang, X. Xia, K. Zhang, Y. Wang, M. Wu, et al., Preventing BRCA1/ ZBRK1 repressor complex binding to the GOT2 promoter results in accelerated

- aspartate biosynthesis and promotion of cell proliferation, Mol. Oncol. 13 (2019)
- [67] T. Corsello, N. Komaravelli, A. Casola, Role of hydrogen sulfide in NRF2- and sirtuin-dependent maintenance of cellular redox balance, Antioxidants (2018), https://doi.org/10.3390/ANTIOX7100129.
- [68] K. Itoh, T. Chiba, S. Takahashi, T. Ishii, K. Igarashi, Y. Katoh, et al., An Nrf2/small Maf heterodimer mediates the induction of phase II detoxifying enzyme genes through antioxidant response elements, Biochem. Biophys. Res. Commun. 236 (1997) 313–322.
- [69] C. Escartin, S.J. Won, C. Malgorn, G. Auregan, A.E. Berman, P.C. Chen, et al., Nuclear factor erythroid 2-related factor 2 facilitates neuronal glutathione synthesis by upregulating neuronal excitatory amino acid transporter 3 expression, J. Neurosci. 31 (2011) 7392.
- [70] S. Song, V. Nguyen, T. Schrank, K. Mulvaney, V. Walter, D. Wei, et al., Loss of SWI/SNF chromatin remodeling alters NRF2 signaling in non-small cell lung carcinoma, Mol. Cancer Res. 18 (2020) 1777–1788.
- [71] J. Jin, F. Chen, W. He, L. Zhao, B. Lin, D. Zheng, et al., YAP-activated SATB2 is a coactivator of NRF2 that amplifies antioxidative capacity and promotes tumor progression in renal cell carcinoma, Cancer Res. (2023), https://doi.org/ 10.1158/0008-5472.CAN-22-1693.
- [72] X. Hu, Y. Zhang, H. Wang, Y. Han, Z. Tian, X. Zhang, et al., BRD9 facilitates oncogenic Nrf2 pathway and dampens venetoclax sensitivity by remodeling chromatin accessibility in chronic lymphocytic leukemia, Blood 140 (2022) 356–357.
- [73] S.A. Leachman, O.M. Lucero, J.E. Sampson, P. Cassidy, W. Bruno, P. Queirolo, et al., Identification, genetic testing, and management of hereditary melanoma, Cancer Metastasis Rev. 36 (2017) 77.
- [74] P. Rentzsch, D. Witten, G.M. Cooper, J. Shendure, M. Kircher, CADD: predicting the deleteriousness of variants throughout the human genome, Nucleic Acids Res. 47 (2019) D886–D894.
- [75] H.A. Shihab, J. Gough, M. Mort, D.N. Cooper, I.N.M. Day, T.R. Gaunt, Ranking non-synonymous single nucleotide polymorphisms based on disease concepts, Hum. Genomics (2014), https://doi.org/10.1186/1479-7364-8-11.
- [76] J.I. Takeda, S. Fukami, A. Tamura, A. Shibata, K. Ohno, IntSplice2: prediction of the splicing effects of intronic single-nucleotide variants using LightGBM modeling, Front. Genet. (2021), https://doi.org/10.3389/FGENE.2021.701076.
- [77] F.O. Desmet, D. Hamroun, M. Lalande, G. Collod-Bëroud, M. Claustres, C. Béroud, Human Splicing Finder: an online bioinformatics tool to predict splicing signals, Nucleic Acids Res. (2009), https://doi.org/10.1093/NAR/GKP215.
- [78] R. Steinhaus, S. Proft, M. Schuelke, D.N. Cooper, J.M. Schwarz, D. Seelow, MutationTaster2021, Nucleic Acids Res. 49 (2021) W446–W451.
- [79] D. Tamborero, C. Rubio-Perez, J. Deu-Pons, M.P. Schroeder, A. Vivancos, A. Rovira, et al., Cancer Genome Interpreter annotates the biological and clinical relevance of tumor alterations, Genome Med. (2018), https://doi.org/10.1186/ S13073-018-0531-8.
- [80] Y. Choi, A.P. Chan, PROVEAN web server: a tool to predict the functional effect of amino acid substitutions and indels, Bioinformatics 31 (2015) 2745–2747.
- [81] K.L. Howe, P. Achuthan, J. Allen, J. Allen, J. Alvarez-Jarreta, M. Ridwan Amode, et al., Ensembl 2021, Nucleic Acids Res. 49 (2021) D884–D891.
- [82] J.G. Tate, S. Bamford, H.C. Jubb, Z. Sondka, D.M. Beare, N. Bindal, et al., COSMIC: the catalogue of somatic mutations in cancer, Nucleic Acids Res. 47 (2019) D941–D947.
- [83] C. Kopanos, V. Tsiolkas, A. Kouris, C.E. Chapple, M. Albarca Aguilera, R. Meyer, et al., VarSome: the human genomic variant search engine, Bioinformatics 35 (2019) 1978–1980
- [84] M. Bespalov, M. Einhorn, A. Kamshov, A. Sheffer, Franklin Genoox. Franklin by Genoox. https://franklin.genoox.com, 2021.
- Genoox. https://franklin.genoox.com, 2021.
 [85] I. Santos, C. Ramos, C. Mendes, C.O. Sequeira, C.S. Tomé, D.G.H. Fernandes, et al., Targeting glutathione and cystathionine β-synthase in ovarian cancer treatment by selenium-chrysin polyurea dendrimer nanoformulation, Nutrients (2019), https://doi.org/10.3390/NU11102523.
- [86] C. Mendes, F. Lopes-Coelho, C. Ramos, F. Martins, I. Santos, A. Rodrigues, et al., Unraveling FATP1, regulated by ER-β, as a targeted breast cancer innovative therapy, Sci. Rep. (2019), https://doi.org/10.1038/S41598-019-50531-3.
- [87] S.C. Nunes, C. Ramos, I. Santos, C. Mendes, F. Silva, J.B. Vicente, et al., Cysteine boosts fitness under hypoxia-mimicked conditions in ovarian cancer by metabolic reprogramming, Front. Cell Dev. Biol. (2021), https://doi.org/10.3389/ FCELL_2021.722412.
- [88] J. Serpa, P. Mesquita, N. Mendes, C. Oliveira, R. Almeida, F. Santos-Silva, et al., Expression of Lea in gastric cancer cell lines depends on FUT3 expression regulated by promoter methylation, Cancer Lett. 242 (2006) 191–197.
- [89] L.S. Silva, L.G. Goncalves, F. Silva, G. Domingues, V. Maximo, J. Ferreira, et al., STAT3:FOXM1 and MCT1 drive uterine cervix carcinoma fitness to a lactate-rich microenvironment, Tumour Biol. 37 (2016) 5385–5395.
- [90] D.N. Hu, Methodology for evaluation of melanin content and production of pigment cells in vitro, Photochem. Photobiol. 84 (2008) 645–649.
- [91] M.J. Hall, S. Lopes-Ventura, M.V. Neto, J. Charneca, P. Zoio, M.C. Seabra, et al., Reconstructed human pigmented skin/epidermis models achieve epidermal pigmentation through melanocore transfer, Pigment Cell Melanoma Res. 35 (2022) 425–435.
- [92] P. Zoio, S. Lopes-Ventura, A. Oliva, Barrier-on-a-chip with a modular architecture and integrated sensors for real-time measurement of biological barrier function, Micromachines 12 (2021) 816.
- [93] U. Uslu, S. Schliep, K. Schliep, M. Erdmann, H.U. Koch, H. Parsch, et al., Comparison of the serum tumor markers S100 and melanoma-inhibitory activity (MIA) in the monitoring of patients with metastatic melanoma receiving

- vaccination immunotherapy with dendritic cells, Anticancer Res. 37 (2017) 5033–5037
- [94] R. Harpio, R. Einarsson, S100 proteins as cancer biomarkers with focus on S100B in malignant melanoma, Clin. Biochem. 37 (2004) 512–518.
- [95] A. Auton, G.R. Abecasis, D.M. Altshuler, R.M. Durbin, D.R. Bentley, A. Chakravarti, et al., A global reference for human genetic variation, Nature 526 (2015) 68–74
- [96] K.J. Karczewski, L.C. Francioli, G. Tiao, B.B. Cummings, J. Alföldi, Q. Wang, et al., The mutational constraint spectrum quantified from variation in 141,456 humans, Nat 5817809 (581) (2020) 434–443.
- [97] S. Bamford, E. Dawson, S. Forbes, J. Clements, R. Pettett, A. Dogan, et al., The COSMIC (Catalogue of Somatic Mutations in Cancer) database and website, Br. J. Cancer 91 (2004) 355.
- [98] D. Dankort, D.P. Curley, R.A. Cartlidge, B. Nelson, A.N. Karnezis, W.E. Damsky, et al., BRafV600E cooperates with Pten silencing to elicit metastatic melanoma, Nat. Genet. 41 (2009) 544.
- [99] M.Y. Hsu, F.E. Meier, M. Nesbit, J.Y. Hsu, P. Van Belle, D.E. Elder, et al., E-cadherin expression in melanoma cells restores keratinocyte-mediated growth control and down-regulates expression of invasion-related adhesion receptors, Am. J. Pathol. 156 (2000) 1515–1525.
- [100] S.C. Nunes, J. Serpa, Glutathione in ovarian cancer: a double-edged sword, Int. J. Mol. Sci. (2018), https://doi.org/10.3390/IJMS19071882.
- [101] N. Nagahara, M. Tanaka, Y. Tanaka, T. Ito, Novel characterization of antioxidant enzyme, 3-mercaptopyruvate sulfurtransferase-knockout mice: overexpression of the evolutionarily-related enzyme rhodanese, Antioxidants (Basel, Switzerland) (2019), https://doi.org/10.3390/ANTIOX8050116.
- [102] A. Giuffrè, J.B. Vicente, Hydrogen sulfide biochemistry and interplay with other gaseous mediators in mammalian physiology, Oxidative Med. Cell. Longev. (2018), https://doi.org/10.1155/2018/6290931.
- [103] J.M. Matés, C. Pérez-Gómez, I.N. De Castro, M. Asenjo, J. Márquez, Glutamine and its relationship with intracellular redox status, oxidative stress and cell proliferation/death, Int. J. Biochem. Cell Biol. 34 (2002) 439–458.
- [104] M. Sahuri-Arisoylu, R.R. Mould, N. Shinjyo, S.W.A. Bligh, A.V.W. Nunn, G. W. Guy, et al., Acetate induces growth arrest in colon cancer cells through modulation of mitochondrial function, Front. Nutr. 8 (2021), 588466.
- [105] J.R. Moffett, N. Puthillathu, R. Vengilote, D.M. Jaworski, A.M. Namboodiri, Acetate revisited: a key biomolecule at the Nexus of metabolism, epigenetics, and oncogenesis – part 2: acetate and ACSS2 in health and disease, Front. Physiol. 11 (2020) 1451.
- [106] N. Mori, F. Wildes, T. Takagi, K. Glunde, Z.M. Bhujwalla, The tumor microenvironment modulates choline and lipid metabolism, Front. Oncol. 6 (2016) 262.
- [107] M. Bagnoli, A. Granata, R. Nicoletti, B. Krishnamachary, Z.M. Bhujwalla, R. Canese, et al., Choline metabolism alteration: a focus on ovarian cancer, Front. Oncol. 6 (2016) 153.
- [108] J. Meiser, A. Schuster, M. Pietzke, J. Vande Voorde, D. Athineos, K. Oizel, et al., Increased formate overflow is a hallmark of oxidative cancer, Nat. Commun. (2018), https://doi.org/10.1038/S41467-018-03777-W.
- [109] K.G. de la Cruz-López, L.J. Castro-Muñoz, D.O. Reyes-Hernández, A. García-Carrancá, J. Manzo-Merino, Lactate in the regulation of tumor microenvironment and therapeutic approaches, Front. Oncol. 9 (2019) 1143.
- [110] A. Napolitano, L. Panzella, G. Monfrecola, M. d'Ischia, Pheomelanin-induced oxidative stress: bright and dark chemistry bridging red hair phenotype and melanoma, Pigment Cell Melanoma Res. 27 (2014) 721–733.
- [111] M.R. Chedekel, S.K. Smith, P.W. Post, A. Pokora, D.L. Vessell, Photodestruction of pheomelanin: role of oxygen, Proc. Natl. Acad. Sci. U. S. A. 75 (1978) 5395–5399.
- [112] L. Panzella, G. Szewczyk, M. D'Ischia, A. Napolitano, T. Sarna, Zinc-induced structural effects enhance oxygen consumption and superoxide generation in synthetic pheomelanins on UVA/visible light irradiation, Photochem. Photobiol. 86 (2010) 757–764.
- [113] E. Wenczl, G.P. Van Der Schans, L. Roza, R.M. Kolb, A.J. Timmerman, N.P. M. Smit, et al., (Pheo)melanin photosensitizes UVA-induced DNA damage in cultured human melanocytes, J. Invest. Dermatol. 111 (1998) 678–682.
- [114] D.N. Hu, K. Wakamatsu, S. Ito, S.A. McCormick, Comparison of eumelanin and pheomelanin content between cultured uveal melanoma cells and normal uveal melanocytes, Melanoma Res. 19 (2009) 75–79.
- [115] D. Hanahan, Hallmarks of cancer: new dimensions, Cancer Discov. 12 (2022) 31–46.
- [116] F. Augsburger, C. Szabo, Potential role of the 3-mercaptopyruvate sulfurtransferase (3-MST)-hydrogen sulfide (H2S) pathway in cancer cells, Pharmacol. Res. (2020), https://doi.org/10.1016/J.PHRS.2018.11.034.
- [117] A.A. Untereiner, A. Pavlidou, N. Druzhyna, A. Papapetropoulos, M.R. Hellmich, C. Szabo, Drug resistance induces the upregulation of H2S-producing enzymes in HCT116 colon cancer cells, Biochem. Pharmacol. 149 (2018) 174–185.
- [118] E.A. Ostrakhovitch, S. Akakura, R. Sanokawa-Akakura, S. Goodwin, S. Tabibzadeh, Dedifferentiation of cancer cells following recovery from a potentially lethal damage is mediated by H2S-Nampt, Exp. Cell Res. 330 (2015) 135–150.
- [119] G. Oláh, K. Módis, G. Törö, M.R. Hellmich, B. Szczesny, C. Szabo, Role of endogenous and exogenous nitric oxide, carbon monoxide and hydrogen sulfide

- in HCT116 colon cancer cell proliferation, Biochem. Pharmacol. 149 (2018) 186–204.
- [120] B. Szczesny, M. Marcatti, J.R. Zatarain, N. Druzhyna, J.E. Wiktorowicz, P. Nagy, et al., Inhibition of hydrogen sulfide biosynthesis sensitizes lung adenocarcinoma to chemotherapeutic drugs by inhibiting mitochondrial DNA repair and suppressing cellular bioenergetics, Sci. Rep. (2016), https://doi.org/10.1038/SREP36125.
- [121] V. Knethen, S. Sousa Santos, L. de Oliveira Cavalcanti Peres Rodrigues, V. Martins, M. Petrosino, K. Zuhra, et al., Role of cystathionine & beta;-synthase and 3-mercaptopyruvate sulfurtransferase in the regulation of proliferation, migration, and bioenergetics of murine breast cancer cells, Antioxidants 12 (2023) 647.